JOURNAL OF MATERIALS SCIENCE **36** (2001) 3833–3854

Review
Grain and subgrain characterisation by electron backscatter diffraction

F. J. HUMPHREYS
Manchester Materials Science Centre, UMIST/University of Manchester, Grosvenor Street, Manchester M1 7HS, UK
E-mail: john.humphreys@umist.ac.uk

The application of automated Electron Backscatter Diffraction (EBSD) in the scanning electron microscope, to the quantitative analysis of grain and subgrain structures is discussed and compared with conventional methods of quantitative metallography. It is shown that the technique has reached a state of maturity such that linescans and maps can routinely be obtained and analysed using commercially available equipment and that EBSD in a Field Emission SEM (FEGSEM) allows quantitative analysis of grain/subgrains as small as $\sim$0.2 μm. EBSD can often give more accurate measurements of grain and subgrain size than conventional imaging methods, often in comparable times. Subgrain/cell measurements may be made more easily than in the TEM although the limited angular resolution of EBSD may be problematic in some cases. Additional information available from EBSD and not from conventional microscopy, gives a new dimension to quantitative metallography. **Texture** and its correlation with grain or subgrain size, shape and position are readily measured. **Boundary misorientations**, which are readily obtainable from EBSD, enable the distribution of boundary types to be determined and CSL boundaries can be identified and measured. The spatial distribution of **Stored Energy** in a sample and the amount of **Recrystallization** may also be measured by EBSD methods.

1. Introduction

The characterisation and measurement of grain and subgrain structures in metals is of great importance to Materials Scientists because not only does the grain size strongly affect the mechanical properties at low and high temperatures, but it has an influence on physical properties, surface properties, phase transformations and annealing behaviour. The grain size, which is a well-defined standard parameter of the microstructure [e.g. 1] and which may be included in materials specifications, has traditionally been measured by optical microscopy [e.g. 2], although scanning electron microscopy (SEM) is increasingly used. For the smallest grain sizes and for subgrain structures, transmission electron microscopy (TEM) may be required, although the problems of preparing and working with the thin specimens required for TEM often make it difficult to measure representative microstructures.

Recent developments in the technique of automated electron backscatter diffraction (EBSD) in the scanning electron microscope which are outlined below, particularly the use of EBSD in conjunction with a field emission scanning electron microscope (FEGSEM), suggest that this technique should now be considered as an important tool for quantitative metallography, and the aim of the present paper is to explore this possibility. The paper considers the application of EBSD to the measurement and characterisation of grain structures and makes comparison with the traditional methods of grain measurement. Because this is a new approach to grain characterisation, there are several aspects concerning the precision of the measurements which require consideration. There are also a number of important microstructural parameters which are now routinely available from EBSD analysis but which are not obtainable from conventional methods of grain characterisation, in particular, parameters relating to the grain orientations and boundary character. As EBSD becomes more widely used, it is likely that some of these parameters will become routinely used to quantify microstructures. This paper will concentrate on the analysis of single-phase materials, although similar principles may be used to quantify the sizes, volume fraction and texture distributions in duplex alloys [3–5]

This paper is concerned with the application of EBSD to various practical problems in Materials Science and does not consider the formal crystallography or physics relating to the acquisition or solution of the diffraction patterns. Detailed treatments of these and other aspects of EBSD are discussed by Wilkinson and Hirsch [6] and in a recent book by Randle and Engler [7]. Currently available equipment and software is such that

the user can usually obtain useful metallographic data from EBSD with little knowledge of the acquisition and data processing methods. However, in order to obtain the maximum amount of information and to be aware of the accuracy and limitations of the technique, it is important that the user is aware of the main principles underlying EBSD.

2. The EBSD Technique

2.1. The method

Electron backscattered diffraction (EBSD) is based on the acquisition of diffraction patterns from bulk samples in the scanning electron microscope, and although such patterns were first obtained over 40 years ago [8] it was the work of Dingley [9] who pioneered the use of low light TV cameras for pattern acquisition and on-line pattern solution, which stimulated widespread interest in the technique, leading to the development of commercially available systems. The development of the EBSD technique up to 1992 is reviewed by Randle [10], and more recent reviews include those of Adams [11], Field [12] and Randle and Engler [7].

Of particular importance in the emergence of EBSD as a metallographic technique was the development of rapid automated pattern analysis [13–15], and this when used in conjunction with control of the microscope beam or stage has enabled line or area scans of a sample surface to be obtained rapidly and automatically. The term "orientation imaging microscopy" or OIM has been used to describe the area scans of a sample [13], although the terms "orientation map" or "EBSD map" which are in common use will be adopted in this article. A more recent innovation has been the use of EBSD in conjunction with Field Emission Gun Scanning Electron Microscopes (FEGSEM) [16], and the consequent increase in spatial resolution has further extended the range of applications of EBSD.

The basic requirement is a scanning electron microscope and an EBSD system. For the highest spatial resolutions a FEGSEM instrument is required and the advantages of such instruments are discussed later. The EBSD acquisition hardware generally comprises a sensitive CCD camera, and an image processing system for pattern averaging and background subtraction. Fig. 1 is a schematic diagram showing the main components of an EBSD system. The EBSD acquisition software will control the data acquisition, solve the diffraction patterns and store the data. Further software is required to analyse, manipulate and display the data. EBSD systems are now widely available from commercial manufacturers, and the method of interfacing an EBSD system to the SEM and its cost are comparable with the cost of an EDX analysis system such as is attached to most SEMs.

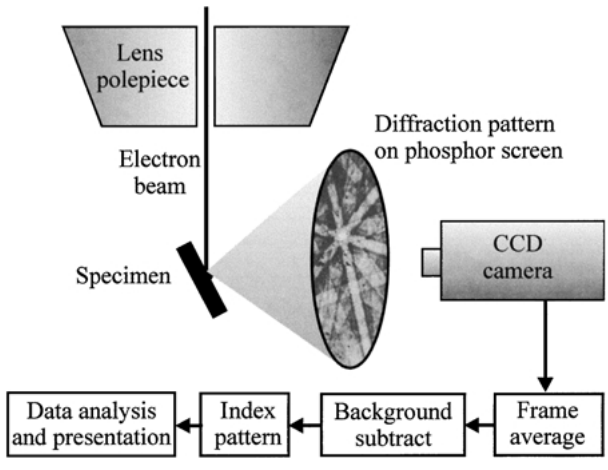

Figure 1 Schematic diagram of a typical EBSD installation.

EBSD is carried out on a specimen which is tilted between 60° and 70° from the horizontal. This is best achieved by mounting the specimen so that the surface is normal to the electron beam, which is the optimum position for examining the microstructure using backscattered electrons. Following such examination the specimen may then be tilted to the EBSD operating position. If a backscattered image is required from the tilted sample, additional backscattered electron detectors must be used [17, 18] and these are typically positioned close to the transmission phosphor screen.

The original and most common application of EBSD is the determination of the local relationships between microstructure and crystallography. For example, a direct correlation between the orientations of the grains in which some particular event is occurring, such as fracture, oxidation, precipitation or recrystallization, or correlation between grain boundary crystallography and properties such as boundary mobility, diffusivity, resistance to chemical attack, mechanical properties etc. Such investigations often enable a better understanding of these phenomena to be obtained. In some cases these investigations do not require fully automated EBSD equipment, because only a few orientation measurements at specific points of the microstructure may be required. A large body of information on such applications is rapidly emerging and can be found in the relevant literature and in reviews [7, 11, 12].

EBSD is also becoming increasingly used for phase identification or crystal structure determination and for this type of work a very high quality diffraction pattern is required and this is normally acquired via a slow scan CCD camera. An automated routine is then used to extract the positions and widths of the bands in the diffraction pattern and the unit cell volume is calculated. This information, coupled with chemical information obtained by EDX microanalysis is then used to search a database of crystal structures [19].

The data required for quantitative microstructural analysis using EBSD is usually obtained in the form of an orientation map (Fig. 2a), although linescans may also be used as discussed below, for such applications, a large amount of data need to be collected in the shortest possible time and the critical parameters are the **speed** of data acquisition and the **spatial** and **angular** resolutions. These depend on a number of factors including the specimen, the equipment and the method of operation. The results presented in this paper were obtained on three instruments in the Manchester Materials Science Centre, a W-filament SEM (JEOL 6300), and two Field Emission Gun SEMs (Philips XL30 and CAMSCAN Maxim 2040SF). All instruments were equipped

with a CCD camera capable of on-chip integration (NORDIF) and the *CHANNEL* EBSD system (HKL Technology, Denmark) with beam and stage control. Subsequent data analysis and presentation were carried out using *VMAP*, an in-house software development [20] and *ICE* (HKL Technology). It should be noted that the microscopes and EBSD acquisition systems are all standard commercially available equipment with no significant modifications. In order to discuss the application of EBSD to quantitative metallography it is first necessary to consider the type, quantity and quality of the data which can be obtained, and a short discussion of the factors which influence these parameters is therefore required.

2.1.1. Beam scanning

In beam scanning mode the normal microscope scan is disabled and the beam is controlled by the EDSD acquisition software. The advantages of this mode of operation are that it is simple and requires no modifications to the microscope and that it is rapid because the time required to move the beam is negligible. The disadvantages are that during the scan, the beam moves off the optic axis and this can result in inaccuracy in the determination of absolute orientations and in beam defocus. Except at very low magnifications the inaccuracy in determining the absolute orientations is typically only $\sim 1^\circ$ at the edges of the scan [21] and this is usually not significant for the applications discussed in this paper, and in principle the data could if required, be software corrected for this effect. A more serious error may arise from defocus of the electron beam as it is deflected perpendicular to the axis of tilt [21]. This effect will be minimised by the use of a "dynamic focus" correction in the SEM, which automatically alters the focus during the scan raster. However, in some instruments the dynamic focus correction may not be compatible with the external beam control required by the EBSD acquisition system. Again, any errors will be minimised at high magnifications and at long working distances.

2.1.2. Stage scanning

In stage scanning mode a stationary electron beam is used and the specimen is moved relative to the beam with stage stepping motors controlled by the EBSD software. With stage scanning the problem of beam defocus is eliminated if the sample surface is accurately aligned with the x–y plane of the specimen stage, and because the beam remains on-axis, the accuracy of the absolute orientation determinations are also maintained. The disadvantage of stage scanning is that it is slower than beam scanning, and the time for stage movement, which depends on the size of the scan steps is typically ~ 1 second. In addition, the positional accuracy of stage scanning using a normal SEM stage is not high, and stage scanning is most suitable for scan steps larger than $\sim 1\ \mu$m.

2.2. Practical considerations

There are a number of factors which must be taken into account when deciding if EBSD can be successfully used for a particular investigation.

2.2.1. The specimen

The backscattered electron signal increases with the atomic number (z) of the material. The quality of the diffraction pattern increases with z and the spatial resolution may also improve with increasing z [16, 22]. The results cited in this paper were mainly obtained from aluminium alloys and somewhat better results would be expected from steels or nickel alloys. The diffraction pattern comes from the surface layer and although in many cases an electropolished surface is required, a good mechanical polish is sufficient for hard materials. In multi-phase alloys, preferential polishing of one phase may, because of the large tilt angle, lead to some shadowing by the protruding phase. In order to obtain an analysable diffraction pattern the region of the specimen from which the pattern is obtained must have a single crystallographic orientation (see below). Thus the smallest grain or subgrain size which can be measured is related to the spatial resolution of the technique. Defects such as dislocations may cause the pattern to lose sharpness, but unless this is severe, the pattern will still be analysable.

2.2.2. The speed of data acquisition

The time to acquire a data point during a scan depends on the **slowest** of three operations:

(a) The time required to obtain an analysable diffraction pattern. This depends primarily on the material and microscope operating conditions and is typically 2–4 TV frames (i.e. 0.05–0.2 s)

(b) The time required to analyse the pattern. This depends on the processing speed of the computer, the speed of the pattern-solving algorithm and the number of lines in the pattern required for a solution, and is typically 0.1–0.5 s. Software which recognises that subsequent similar patterns do not require analysis may lead to significant increases in speed.

(c) The time to reposition the beam or stage, which as discussed above is negligible for beam scanning but may be greater than 1 s for stage scanning.

At the time of writing, the average time per data point on our systems for aluminium samples, where we typically average the pattern for 2 frames, is 0.1–0.2 s for beam scanning and ~ 1 s for stage scanning. Some crystal structures require measurement of more diffraction lines for accurate indexing and this increases the data processing time. If it is required to check the solution against more than one possible phase in the material then again this slows down the calculation.

2.2.3. Spatial resolution

If the area of the sample contributing to a diffraction pattern contains more than one crystallographic orientation, e.g. a grain boundary region, a single crystal diffraction pattern is not obtained, the automated pattern solving routines may fail and the pattern will not be indexed. This is clearly seen in the small EBSD map of Fig. 2a, where the colours are chosen to represent the orientations of the pixels and the individual grains are clearly revealed. Non-indexed points, which are black, are seen to occur at some points on the grain boundaries.

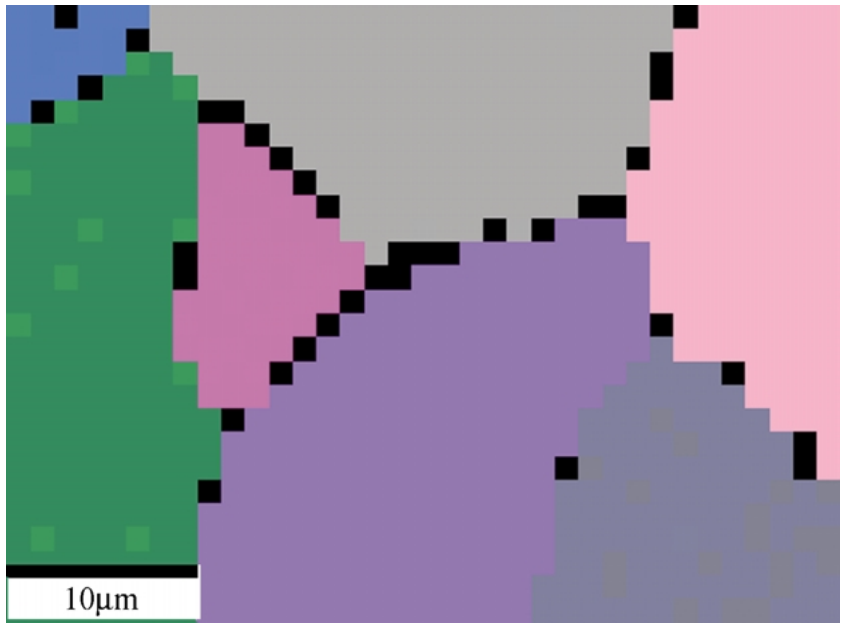

(a)

(b)

Figure 2 Part of an orientation map. (a) Euler contrast in which the red, green and blue intensities are proportional to the three Euler angles defining the pixel orientation. Non-indexed points are black. (b) Pattern quality map of the same area. Boundary regions exhibit lower pattern quality due to pattern overlap.

The area from which an EBSD pattern is acquired with an electron beam focused on a 70° tilted sample is approximately elliptical, with the major axis, which is perpendicular to the tilt axis, being some 3 times that of the minor axis (Fig. 3). It is a function of material, beam accelerating voltage, specimen tilt and probe size, and the resolution parallel to the tilt axis (Λ_A) for a standard W-filament SEM is typically in the region of 200–500 nm [16, 22] for aluminium.

However, when analysing a sample with small grains or subgrains the achievable spatial resolution is rather smaller than this because, when patterns from two grains overlap, the acquisition software can, if there is a significant difference in intensity of the patterns, successfully analyse the stronger pattern. This **effective resolution** may be conveniently determined by measuring the fraction of patterns (N_S) which are solved during a raster scan of the sample, and for grains of mean size D_A and D_P parallel and perpendicular to the tilt axis, N_S is given approximately [23] by

$$N_S = \frac{(D_A - \Lambda_A)(D_P - \Lambda_P)}{D_A D_P} \quad (1)$$

where Λ_A is the effective spatial resolutions parallel to the sample tilt axis and Λ_P the resolution perpendicular to the axis (Fig. 3).

For an equiaxed microstructure of grains of diameter D, and taking $\Lambda_P = 3\Lambda_A$, which is typically found for

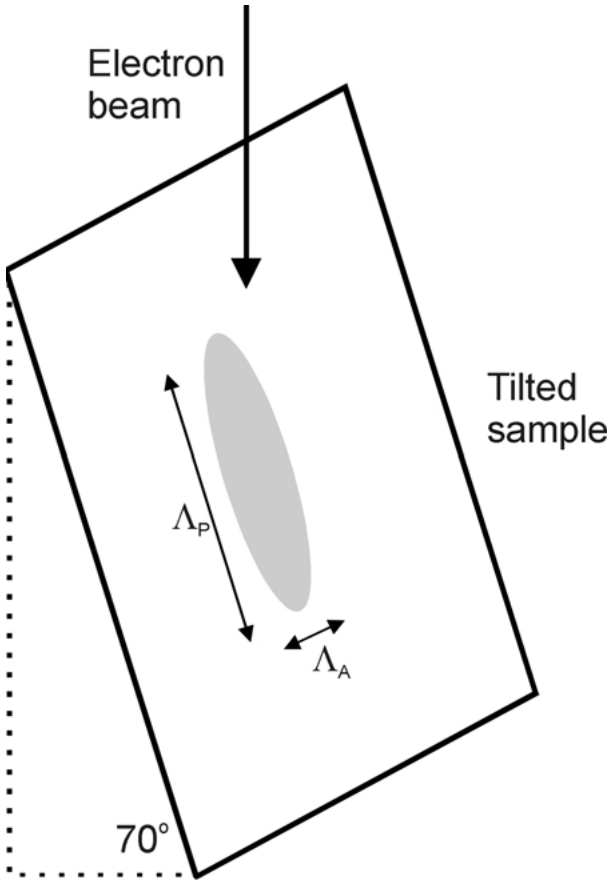

Figure 3 The geometry of the electron beam and the sample.

a 70° tilted sample [23], then when $\Lambda_A \ll D$

$$\Lambda_A = \frac{D(1 - N_S)}{4} \tag{2}$$

These relationships assume that all non-indexing is due to boundaries, which is a reasonable assumption for single-phase materials. However, in a sample containing a volume fraction F_V of a second phase which does not produce indexed patterns, N_S in the above equations should be multiplied by $1/(1 - F_V)$.

Fig. 4a is a plot of N_S against D^{-1} for aluminium samples under optimum operating conditions, and it is seen that the spatial resolution for EBSD in the FEGSEM, which is obtained from the slope of the line, is some 3 times better than in the W-filament SEM. As expected, better spatial resolution is obtained for materials of high atomic number, and data for α-brass in Fig. 2a show the resolution in the FEGSEM to be ~9 nm, which compares to ~25 nm in the W-filament SEM [16].

The effect of beam current on Λ_A is shown in Fig. 4b. For the W-filament SEM, Λ_A is a strong function of the probe current [16, 23]. For small probe currents, the pattern-solving algorithms have difficulty deconvoluting and solving overlapping diffraction patterns of poor quality, whereas at large probe currents the resolution is limited by beam spread in the sample due to the large beam size. Thus the optimum resolution is obtained at intermediate probe currents. It is significant that the resolution of the FEGSEM is much less sensitive to the probe current than the W-filament SEM. This arises because the beam size in a W-filament microscope is a

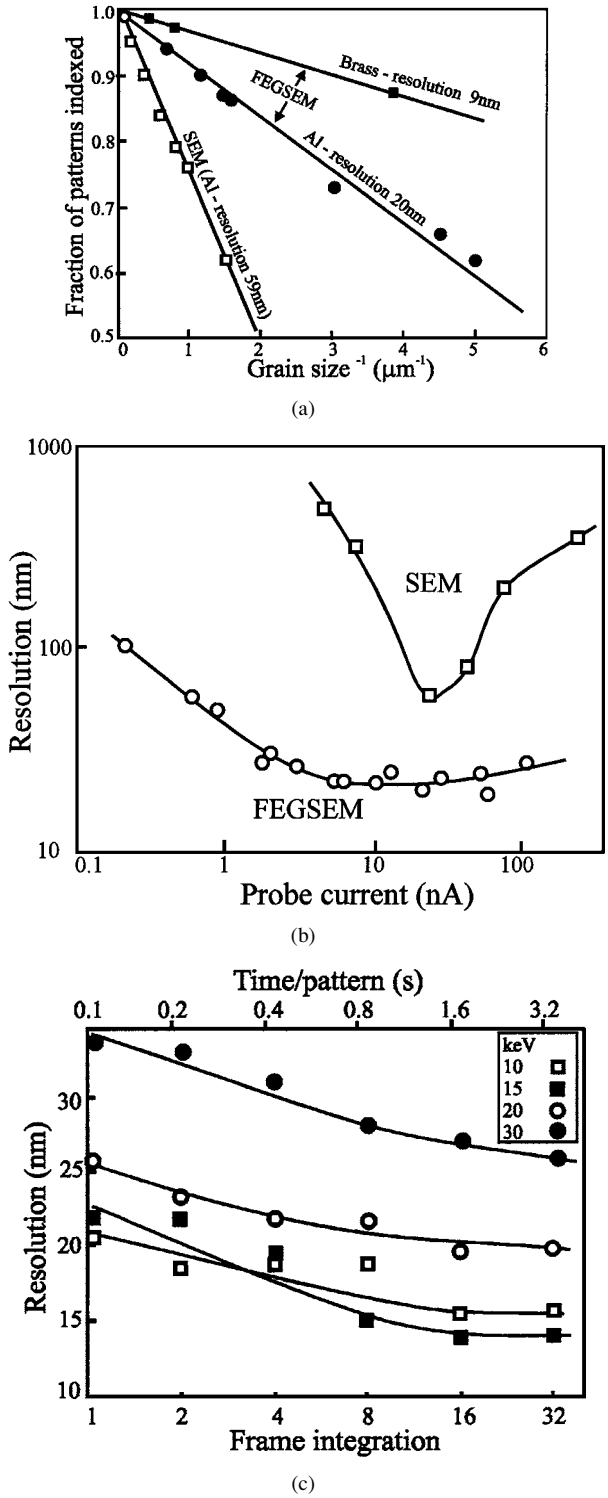

Figure 4 **EBSD** spatial resolution. (a) The effect of grain size on the fraction of diffraction patterns indexed in polycrystalline aluminium alloys and α-brass at 20 keV in a FEGSEM. The results are compared with those obtained in a W-filament SEM. (b) The effect of probe current on the effective spatial resolution in aluminium at 20 keV for a W-filament SEM and a FEGSEM. (c) The effect of accelerating voltage and frame integration on the effective spatial resolution for aluminium at a beam current of ~15 nA [16].

*The probe currents shown in figures 4b and 5b and reported in reference 16 were measured using a Keithley analogue meter. Subsequent measurements of current using a new digital meter have shown the original current readings to be too large and the corrected values are shown in figures 4b and 5b.

much stronger function of probe current than for a field emission gun [24].

There are a number of other factors which affect the EBSD performance as shown in Fig. 4c. As the length of time (or number of frames) over which the pattern is averaged increases, the quality of the pattern and thus the effective spatial resolution improve [16], although the data acquisition time is lengthened. The microscope accelerating voltage also has some effect. The beam spread in the sample increases with accelerating voltage and should therefore be kept as low as possible. However, below ∼15 keV the resolution deteriorates, and this is believed to be the result of a reduction in pattern quality due to a reduction in the efficiency of the transmission phosphor at lower voltages. In practice, an accelerating voltage of ∼20 keV is commonly used. It is to be expected that some improvement in spatial resolution at lower voltages (5–10 keV) will be achievable in the future if the pattern acquisition methods are improved.

2.2.4. Angular precision

The **absolute orientation** of a crystallite is typically obtained with an accuracy of ∼2°, depending on the sample alignment and EBSD operating conditions [e.g. 21]. However, when characterising microstructures containing low angle grain boundaries, the accuracy with which the **relative orientation** between adjacent data points can be determined is of great importance, and this is related to the precision with which the orientations of data points within the same crystallite can be measured. If diffraction patterns are obtained from a small area of a single crystal or a single grain within a large-grained polycrystal, then although their analysis should result in identical orientations, this is not usually the case, and a range of measured orientations results. The resulting "orientation noise" can be quantified in terms of the apparent misorientations between these data points [16, 25, 26]. In a sample in which there are low angle grain boundaries, the measured distribution of misorientations is the sum of the orientation noise and the real misorientation distribution, as shown schematically in Fig. 5a, and therefore very small misorientations are difficult to determine.

Several of the factors which determine the orientation noise, including the number of pixels in the CCD camera, the resolution of the digitised pattern and the accuracy of the pattern solving algorithms, are beyond the direct control of the microscopist. However, it has been shown that the angular resolution is affected by the microscope operating conditions [16, 25], and this effect has been measured for the FEGSEM as shown in Fig. 5b. With increasing probe current, the angular resolution decreases to a constant value which is the limit imposed by the data acquisition system. It is seen that the angular resolution improves at higher accelerating voltages and this is thought to be because the positions of the narrower Kikuchi bands are determined more accurately. It has also been shown that the improvement in angular resolution for larger probe currents is directly related to the increased pattern quality under these conditions. The angular precision may also improve, particularly for poor quality patterns if the number of lines measured from the diffraction pattern is increased [25] although this slows down the data processing rate. If the misorientation between regions in the sample is expressed as an angle-axis pair then for small misorientations, the lack of precision in orientation measurements discussed above will result in a large error in the determination of the misorientation axis [26, 27]. The implications of the limited angular resolution for quantitative metallography are further discussed in Section 3.2.4.

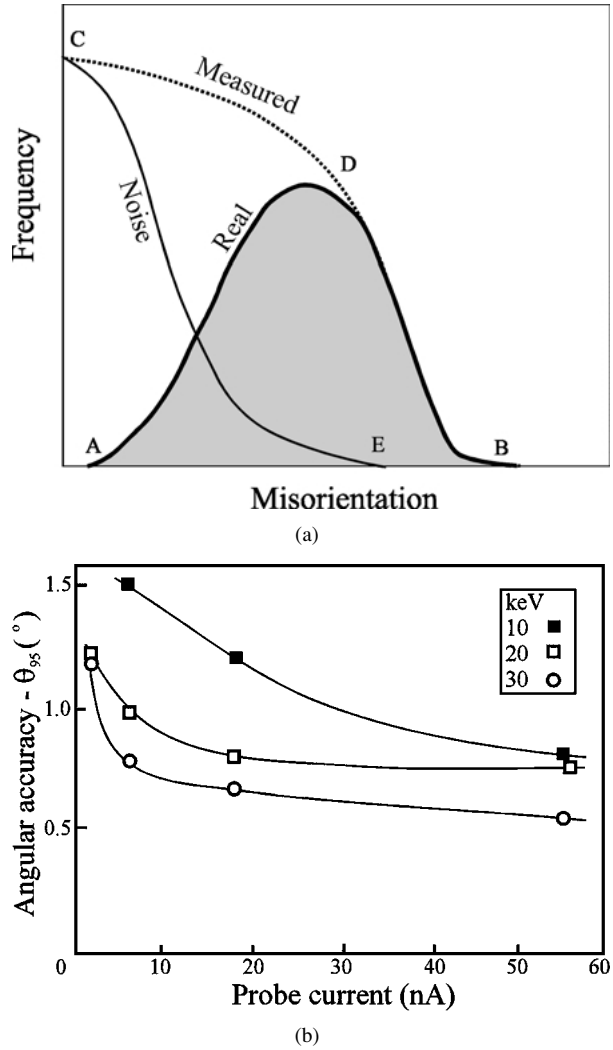

Figure 5 The angular resolution of EBSD. (a) Schematic diagram showing the relationship between the real and measured misorientation distributions and the orientation noise. (b) The effect of probe current on the angular accuracy in the FEGSEM for single grains in a large-grained aluminium sample [16].

2.2.5. Non-indexed data points

Each point on the specimen from which a diffraction pattern is collected does not necessarily produce data because the pattern quality may be too poor to analyse (e.g. a severely deformed region, an inclusion, pit etc.). Alternatively the software may not be able to distinguish between overlapping patterns at grain, subgrain or phase boundaries (e.g. Fig. 2a). If the number of such non-indexed points is large then it may be difficult to obtain quantitative microstructural data, but if the number of non-indexed points is small then the data may be "repaired" by assigning the orientation of a neighbouring point to the non-indexed point. This is similar to

TABLE I Summary of typical EBSD performance for various metals in W-filament and FEG microscopes

Sample and microscope type		Spatial resolution (nm)		Angular precision (degrees)	Time/pattern (s)	
		Λ_A	Λ_P		Beam scan	Stage scan
Aluminium	W	60	180	1	0.2	1
	FEG	20	60	1	0.2	1
Brass	W	25	75	1	0.1-0.2	1
	FEG	9	27	1	0.1-0.2	1
α-iron	W	30	90	1	0.1-0.2	1
	FEG	10	30	1	0.1-0.2	1

the dilation methods used in image analysis software, and some caution should be exercised in using such a procedure. Non-indexing is a particular problem with small grain or subgrain sizes as discussed above, and the consequent limitations on quantitative grain or subgrain measurement are discussed in Section 3.2.2.

2.2.6. Wrongly indexed data points

In some cases the acquisition software may wrongly index a pattern. This is most likely if the diffraction pattern is symmetrical and if the pattern quality is poor. Indexing errors are a particular problem in crystals of low symmetry such as many minerals where pseudosymmetry may limit the use of automatic pattern analysis [28, 29]. In cubic metals, wrong indexing is rare for a well calibrated system and mis-indexed points generally appear as isolated pixels on an orientation map and as they are typically highly misoriented to the adjacent pixels they can often be recognised. The software used for analysing and displaying EBSD data usually allows such points to be removed. The problem is minimised by the use of good quality patterns, accurate calibration and the use of a large number of bands for pattern solution.

2.3. The current status of the technique

Automated EBSD methods have been established for a number of years, and standard systems to fit most SEMs are available. Developments in the near future are likely to be incremental and will lead to some improvements in acquisition time, angular and spatial resolution. However, the technique is now mature and stable and is used in many Materials Research Laboratories ($\sim$1000 World-wide), and we can begin to consider it as a standard technique. Before discussing the application to grain characterisation in detail, it will be useful to summarise typical operating and performance parameters for EBSD, based on our equipment and experience. When routinely acquiring data for quantitative metallography in a standard SEM and using commercially available EBSD equipment, we find that the most relevant parameters which affect the quantity and quality of the data are **material, pattern acquisition time, effective spatial resolution** and **relative angular precision**. These parameters, which are summarised in Table I for W-filament and FEG microscopes will be used as a basis for the discussions which follow.

3. Measuring grain or subgrain size by EBSD

3.1. Strategies

The sizes and shapes of grains in an undeformed metal or ceramic are parameters which are commonly obtained by standard metallographic methods such as optical or scanning electron microscopy, but these may also be obtained by automated EBSD. There are several excellent standard treatments of quantitative metallography [e.g. 2, 30] which discuss the geometrical and statistical basis of grain size measurement, and in this paper some familiarity with the principles of quantitative metallography will be assumed.

As there are a number of ways of both acquiring and analysing the data, a discussion of the possible strategies is required.

3.1.1. Linear intercept method

An orientation map such as shown in Fig. 6 may be obtained from a representative area of the sample. A line of data points in the x-direction is then analysed by comparing the orientations of adjacent points and noting the number of high angle grain boundaries detected along the line. A prior decision as to what misorientation constitutes a high angle boundary must be taken and 15° is often used. The ability to precisely define the nature of the boundaries constitutes a significant advantage over methods such as optical or SEM imaging where the visibility of a boundary is a function of the technique and where all visible boundaries must be measured.

Non-indexing of patterns will sometimes occur at grain boundaries because of pattern overlap, in which case the orientations of the indexed points on either side of the non-indexed point are compared. This will lead to inaccuracy if the amount of non-indexing is such as to cause a complete grain to be missed, although this will only be a serious problem when the grain size is very small as discussed in Section 3.2.2. The data scan is repeated for a new value of y, but not all rows of data are scanned, and in order to avoid oversampling of the data it is usual to repeat the procedure for steps in the y-direction which are no smaller than the grain size. The procedure is repeated for data scans in the y-direction at increasing values of x (Fig. 7), and the mean linear intercept grain size in the x direction (L_X) is then given by:

$$L_X = \frac{R_X P_X \delta}{N_X} \tag{3}$$

where R_X = number of rows scanned in x direction, N_X = number of boundaries intercepted, P_X = number

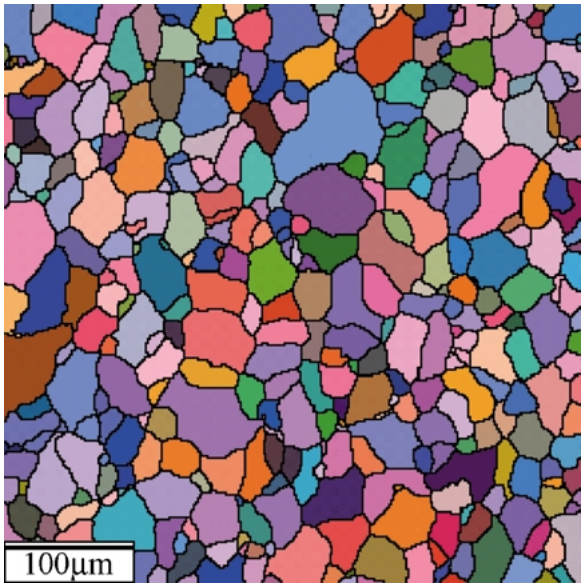

(a)

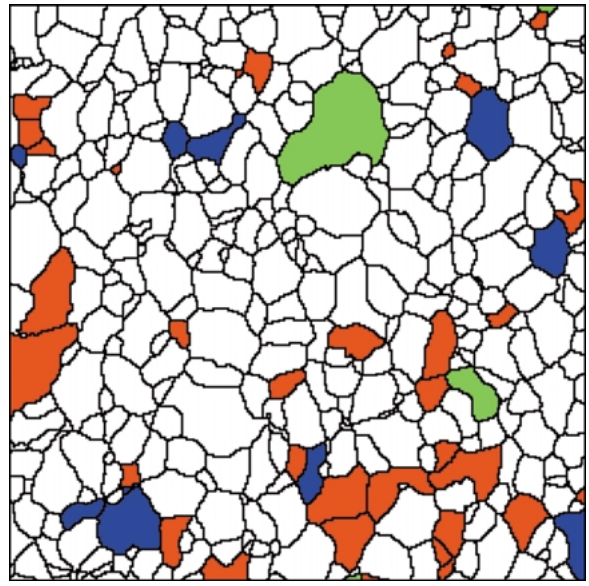

(b)

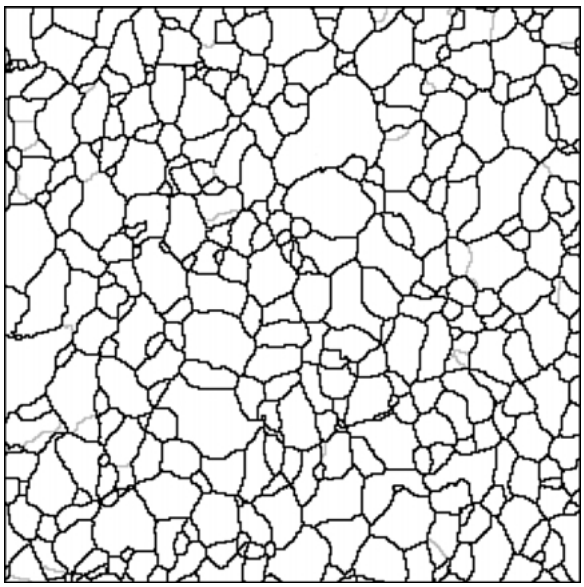

(c)

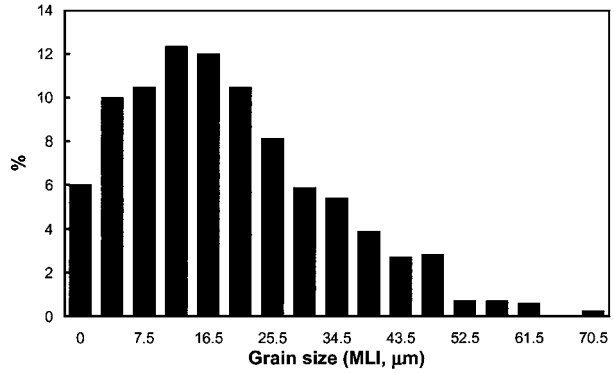

(d)

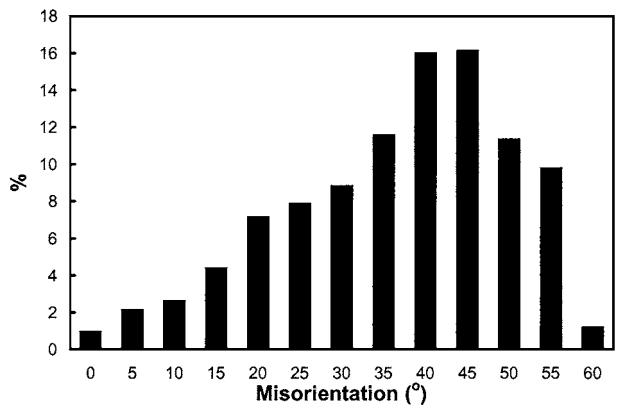

(e)

Figure 6 EBSD map of a recrystallized specimen of a commercial Al-Mg alloy (AA5182) with a weak texture. The specimen has been sectioned in the ND-RD plane. (a) Orientation map where the grains are shown in Euler contrast and high angle grain boundaries are shown as black lines. (b) Grains of the main texture components coloured – Red = *Cube* {100}⟨001⟩, Green = *Goss* {011}⟨100⟩, Blue = *Brass* {011}⟨211⟩. (c) Boundary map with high angle (>15°) grain boundaries shown as black and low angle boundaries as grey. (d) The distribution of grain sizes as measured by linear intercept. (e) The distribution of boundary misorientations as measured by linear intercept.

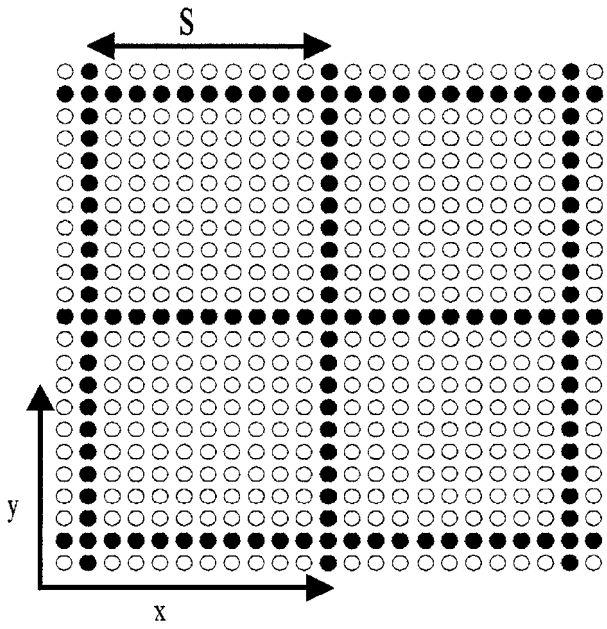

Figure 7 Schematic diagram showing the pixels of an orientation map as open circles and the data set required to measure linear intercept grain sizes as filled circles.

of pixels in x direction, δ = scan step distance between pixels.

The mean linear intercept grain size in the y-direction (L_Y) is similarly calculated, and the overall mean linear intercept ($\bar{L}$) may be obtained from L_X and L_Y. This method of analysis is identical to the standard intercept procedures used to measure grain sizes from optical or scanning electron micrographs. It is of interest to examine the time required for the EBSD method. A minimum number of ~200 grains is typically required for a determination of grain size, and ~5–10 data points across a grain are required to define the grain size with sufficient accuracy (see Section 3.2.1). This suggests that a map of ~20,000 points is required. If this is carried out by beam scanning then this would take ~60 minutes which is a significant amount of instrument time, but as the data acquisition and processing procedures are fully automated, little operator time is required. However, as seen from Fig. 7, only a small fraction of the data in the map are used for such an analysis and a more efficient method of obtaining the data would be to acquire only the data required by scanning the points corresponding to the filled circles of Fig. 7. If the distance S in Fig. 7 is taken to be the grain diameter, the amount of experimental data required is reduced by a factor of 5 and the time taken to acquire the data is reduced to less than 15 minutes. If the data are acquired by stage scanning then as discussed above, these times are increased by a factor of ~4–5. In addition to obtaining the mean linear intercept grain size, the intercept data may also be used to obtain the grain size distribution in the sample as shown in Fig. 6d.

Although the grain size measured by EBSD in a specimen with a weak crystallographic texture is usually found to be similar to that obtained by standard imaging methods such as optical or SEM channelling contrast [21], in a specimen with a strong crystallographic texture it is found that the grain size determined by EBSD is significantly larger than that produced by e.g. SEM imaging [21] as shown in Table II. The reason for this difference arises because all the visible boundaries are measured when an imaging method is used, whereas only the boundaries defined as high angle (e.g. >15°) are measured by EBSD. A strongly textured material has a large fraction of low angle boundaries and therefore SEM backscattered imaging which reveals both high and low angle boundaries gives a smaller grain size than when using EBSD and counting only high angle boundaries. If the EBSD analysis is set to include all the boundaries, then the grain size becomes similar to that measured by SEM imaging as shown in Table II. By using a quantitative definition of a high angle grain boundary, EBSD therefore provides more accurate data than conventional imaging in which the boundaries to be counted depend on the technique used. EBSD provides both the HAGB-only grain size and the HAGB + LAGB grain size, and operator may select that which is most appropriate.

We have discussed a division of boundaries into only two classes—low and high angle boundaries, but the EBSD data contain much more detailed information about the grain boundary misorientations which would not be obtainable from optical or electron microscopy images. For example, in some cases, the microscopist may wish to exclude coherent ($\Sigma 3$) twin boundaries during grain measurement. When standard imaging methods are used, such boundaries are crudely identified by their planarity. However with the use of EBSD the boundaries are characterised and it is therefore possible to include or exclude a particular class of boundary with great accuracy. We see that the additional information available from EBSD adds a new dimension to quantitative metallography, and this is discussed in more detail in Section 4.

3.1.2. Grain reconstruction method

An alternative method of analysing the grain structures from data such as shown in Fig. 6 is by grain reconstruction, in which complete grains are identified. This type of analysis is capable of producing more complete information on grain areas, shapes etc than the intercept method, but because it relies on obtaining a full

TABLE II A comparison of linear intercept grain sizes ($\bar{L}$) measured by various techniques [21]

Sample	Optical imaging (μm)	SEM imaging (μm)	EBSD			
			hagb (μm)	hagb + lagb (μm)	Mean misn (o)	% lagb
AA5182 (weak texture)	25.1	24.8	22.8	21.4	40.3	3
AA5182 (strong texture)	48.5	30.9	52	29.7	22.8	43.3

orientation map, it is considerably slower. This method is related to the image reconstruction methods used in image analysis. Use of grain reconstruction requires careful consideration of how we define a grain. Two different, but equally valid definitions are:

(a) A region containing material which is within a (small) specified orientation range.
(b) A region which is entirely bounded by high angle grain boundaries.

For a randomly oriented assembly of grains there is little difference in the grain sizes determined according to these definitions because ~98% of the boundaries in such an assembly are of high angle (>15°) [31]. However, if the material has a strong crystallographic texture, there will be a significant fraction of low angle boundaries and the grain size measured according to (a) will be smaller than that defined by (b). Similarly, a deformed and recovered polycrystal will contain a large number of low angle boundaries and there will be a large difference between grain sizes (a) and (b).

Grains may be reconstructed to comply with either definition by using absolute or relative referencing. Using absolute referencing, a reference data point or pixel is selected on the map. The misorientations with respect to the reference point, of pixels adjacent to the reference point are determined, and if within a specified limit (Δ_H), these pixels are assigned to the same grain as the reference point. This procedure is then continued until a complete "grain" has been defined [32, 33]. A new reference point which has not already been assigned to a grain is then selected and the process repeated until all the data in the map have been assigned to grains. The reconstruction procedure using relative referencing is similar except that the boundaries of the grain are defined in terms of the misorientation between adjacent pixels.

The differences between absolute and relative reconstruction are illustrated schematically in Fig. 8 in which the orientation variation across a sample is represented by a single parameter (θ). The sample contains a number of low angle boundaries (L) and a high angle boundary (H). If we use absolute referencing, then starting from a reference point at the origin (O) and with Δ_H set to detect high angle boundaries, the grain edge will be detected at A, although this is actually a low angle boundary. This is because the material to the right is misoriented by more than Δ_H from the reference pixel at the origin. The grain which is reconstructed by such a method is consistent with definition (a) but not (b). If we reconstruct with relative referencing then the grain edge is found to be at B and this is consistent with definition (b). EBSD can thus cope with various definitions of grains and the user should select that which is most appropriate to their application.

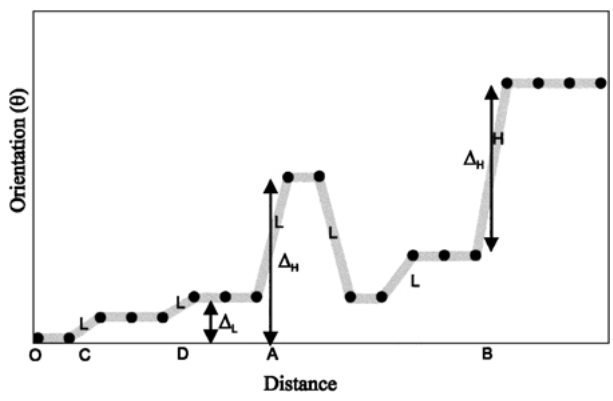

Figure 8 Schematic graph showing the change of orientation with distance, and the method of relative and absolute grain reconstruction.

For the case of a recovered polycrystal containing both grains and subgrains (e.g. Figs 13 and 18) a reasonable definition of a subgrain might be "a region bounded by at least one low angle boundary". Either absolute or relative referencing may be used to detect the boundaries. However, because of the angular resolution limit in EBSD, misorientations below a lower limit (Δ_L) are disregarded and this may cause problems in characterising microstructures with small subgrain misorientations. For example, if we have two adjacent low angle boundaries, both of which are of misorientation $<\Delta_L$ (C and D in Fig. 8) then using relative referencing, neither boundary would be detected, but using absolute referencing a boundary would be detected at D. For low misorientation subgrain structures it may therefore be preferable to use absolute referencing.

Using reconstructed grains, the size of a grain or subgrain is obtained from the number of data points or pixels in the grain, and, using the known pixel step size, the grain area (A) is calculated. The most convenient measure of grain size from such a knowledge of the grain area is the "Equivalent Circle Diameter" or ECD, which is the diameter of a circle having the same area, and this is appropriate for equiaxed grains.

The ECD is related to the true grain diameter $\bar{D}$ [2, 34] by:

$$\text{ECD} = 0.816\bar{D} \tag{4}$$

and to the mean linear intercept ($\bar{L}$) by:

$$\text{ECD} = 1.224\bar{L} \tag{5}$$

The raw data need to be corrected for edge effects using standard methods of quantitative metallography, and a correction must be made for non-indexed data points if these have not been "removed" during data processing as discussed earlier (Section 2.2.5). The simplest correction for an indexed fraction of points N_S, is to take the real grain area as A/N_S. However, a large amount of non-indexing may introduce other systematic errors as discussed in Section 3.2.

The advantages of grain or subgrain reconstruction are that extensive information is obtained about the grains, including area, ECD, Feret diameters and aspect ratios. In addition to orientation, the orientation of a grain or subgrain with respect to all its (visible) neighbours is known and subgrain misorientations (which can be defined as the mean misorientation between a subgrain and its contiguous subgrains [35]), can be measured.

3.1.3. Intelligent data acquisition

Of the methods discussed above, the linear intercept method provides limited data and the grain reconstruction method tends to be slow. Grain reconstruction is

slower than necessary because most of the data acquired during an EBSD scan is redundant. For example if we acquire ten pixels across a grain or subgrain then the total number of data points per grain is ~100, most of which are redundant because they are located in the middle of the grain. Other methods of characterising grains in similar detail to reconstruction, but with more efficient data collection are currently being developed. In the technique of Adaptive Orientation Image Microscopy [36], a coarse grid of data points is initially acquired. If the four points bounding a cell of the grid are of the same orientation then it is assumed that this cell contains only one grain and no further data are required within this cell. If the points bounding a cell are not of the same orientation then a higher resolution grid is obtained within the cell etc. It is claimed that such a method can reduce the scan time by a factor of between 5 and 50. Another approach is to use backscattered electron images of the sample to detect the boundaries and to use this information to automatically locate positions for EBSD analysis [37]. Although this method can locate boundaries and triple points rapidly and with great positional accuracy, the contrast mechanisms are such that any imaging method is likely to fail to detect some boundaries [18].

3.2. The Precision of measurement

The accuracy of grain and subgrain sizes determined by automated EBSD will depend on the sample, microscope and modes of data acquisition and analysis.

3.2.1. EBSD step size

If grain or subgrain sizes are to be determined from an EBSD map then consideration must be given to the pixel step size (δ) in relation to the grain size ($\bar{L}$ or ECD). The greatest accuracy will clearly be obtained if δ is small, and as δ is increased, there is an increasing chance of missing grains or grain intercepts and the measured grain size will be larger than the true grain size. The errors involved could be measured experimentally from a series of EBSD maps from the same sample with varying values of δ. However, in order to eliminate any sampling errors which might occur between the various maps, a large map with a very small value of δ can be obtained, and from these data, smaller maps with larger δ may be obtained by systematically removing data points (e.g. 1 in 5, 1 in 4 etc.) and thus constructing maps of the same area with larger step sizes. The results of such a procedure are shown in Fig. 9, which was obtained for a single-phase aluminium alloy containing grains of ECD ~30 μm. The errors in both mean linear intercept grain size and ECD are plotted. These show that to obtain an accuracy of 10% at least 5 pixels per grain are required, and for an accuracy of 5%, a minimum of ~8 pixels per grain are required.

3.2.2. Measuring small grains and subgrains—the effects of non-indexed points

Although the methods of characterising grains or subgrains by EBSD are simple in principle, problems will arise when the size approaches the limit of **spatial** resolution for EBSD and when the subgrain misorientations approach the limit of **angular** resolution of EBSD. The latter factor will be discussed in the next section, but some further discussion is required of the effects of spatial resolution on the determination of the sizes of small grains or subgrains.

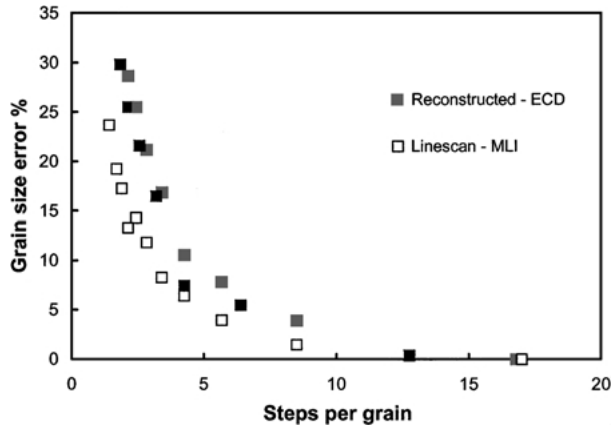

Figure 9 The effect of pixel step size on the accuracy of grain size measurement using linescan and grain reconstruction.

It was shown in Section 2.2.3 (Equations 1 and 2) that there is a simple relationship between the effective spatial resolution, the grain size, and the fraction of diffraction patterns which can be solved. If we consider an EBSD linescan, in a direction parallel to the specimen tilt axis, of a material with an equiaxed grain structure of mean linear intercept $\bar{L}$, then if $\Lambda_P \ll \bar{L}$, all boundaries on the line will be detected and the measured grain size ($\bar{L}_M$) will be correct. However, as $\bar{L}$ approaches Δ_P, the amount of non-indexing of patterns at boundaries will cause some small boundary segments to be missed and thus the measured linear intercept grain size increases. This effect has been modelled in the computer by superimposing a rectangle of dimension Λ_P by Λ_A (aspect ratio 3:1) on a simulated grain structure, moving this to simulate a line scan and assuming that data points would not index if the rectangle covered a boundary [21]. The variation of $\bar{L}_M$ with Λ_P, for $\Lambda_P/\bar{L} < 0.5$, was found to be given by the empirical equation:

$$\frac{\bar{L}_M}{\bar{L}} = 1 + \frac{\Lambda_P}{\bar{L}} + 2\left(\frac{\Lambda_P}{\bar{L}}\right)^2 \qquad (6)$$

This indicates that the error in determining the grain size is less than 10% if $\bar{L} > 10\Lambda_P$ but then increases rapidly as Λ_P approaches $\bar{L}$. Comparison with Equation 2 shows that the criterion for an error of less than 10% is equivalent to a pattern indexed fraction (N_S) of >0.85.

We therefore expect that the smallest grain or subgrain sizes that can be accurately measured by EBSD by linear intercept analysis in aluminium are ~1.8 μm in a W-filament SEM and ~0.5 μm for a FEGSEM. For a material of higher atomic number, Table I suggests that these figures may be substantially reduced. For materials with small grain sizes the apparent grain

size measured by linear intercept could in principle be corrected by the use of Equation 6.

The discussion above shows that although measurement of grain/subgrain size and misorientation by means of line or grid scans is rapid, errors will occur when $\Lambda_P/\bar{L}$ increases and the fraction of indexed points falls below ~0.85. In such circumstances the use of high resolution EBSD maps which allow the correction of non-indexed points, and grain reconstruction methods, may be preferable because in such maps only the smallest **grains** rather than the smallest **intercepts** are lost. If the real grain size distribution is known then the effects on the mean measured grain size of missing the smaller grains may be calculated. For example a recrystallized metal typically has a grain size distribution which is close to log-normal with the largest grains around three times the mean. If grains of size less than Δ_P are not detected, analysis of the "measured" size distribution suggests an error of less than ~10% if $\bar{L}$ is larger than $\sim 2\Lambda_P$ which corresponds to ~50% of the grains being indexed, and to a lower grain size limit for aluminium of ~0.4 μm in a W-filament microscope and ~0.12 μm in a FEGSEM.

The effect of non-indexing of patterns on the measured grain size may also be estimated by taking an EBSD map of a recrystallized grain structure which is well indexed (e.g. >95%) and deliberately de-indexing pixels in the vicinity of grain boundaries. This allows the effect of indexing to be studied on the same data set, although there is some uncertainty as to how well the artificial de-indexing mimics the real situation. The results of such a procedure are shown in Fig. 10, which is based on data from an EBSD map of a single-phase aluminium sample with a grain size of ~25 μm which was 97% indexed. The important points to note are that for the raw data, the error in determining the mean linear intercept grain size corresponds reasonably well to Equation 6 and shows that substantial errors occur if the indexing is less than ~85%. However, if the non-indexed points are restored by the standard EBSD data analysis routines, then the errors in grain size (both linear intercept and ECD) are substantially less, and remain below ~5% even when the indexing is only 50%.

It should be emphasised that the discussions above relate to data from single-phase polycrystalline materials where all non-indexing arises from diffraction pattern overlap at grain boundaries. If the presence of second-phases leads to additional non-indexing, then this must be taken into account as discussed in Section 2.2.5.

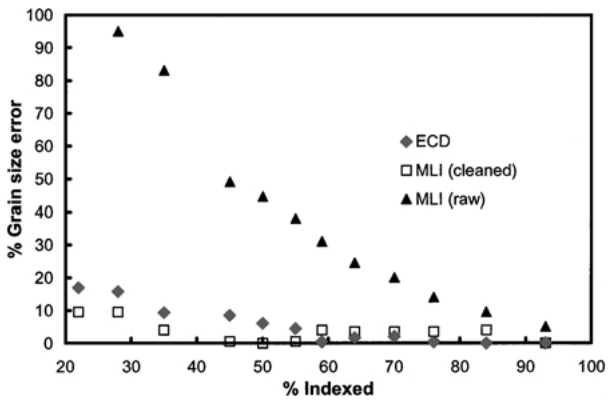

Figure 10 The effect of non-indexed points on the accuracy of grain size measurement by linear intercept analysis of the data and from grain reconstruction.

3.2.3. Other errors in grain size measurement

In the preceding sections we have discussed the methods of grain size measurement by EBSD and the inherent advantages and limitations of the technique. There are however, a number of other factors which must be taken into account if accurate results are to be obtained.

Instrument calibration. The scan rasters used for EBSD are generated by either beam or stage scanning. Care must be taken that the scan distances are accurately calibrated and that the x and y scans are orthogonal. International standards for scanning electron microscopy are not yet available, although standards for the calibration of the magnification of the SEM are being developed (ISO 16700) [38].

Specimen tilt axis. The specimen tilt axis must be accurately aligned with one of the scan directions otherwise a distorted scan raster will result.

Sample alignment. The surface of the sample must be planar and accurately parallel to the x–y plane of the stage (i.e. normal to the electron beam). A sample is typically supported either on its base or is gripped by its sides and as samples are rarely cut in the form of orthogonal parallelepipeds, it may be difficult to align the top surface accurately. If this is not achieved, then the inaccuracies in the scan raster on a 70° tilted sample may be substantial and render quantitative metallography impossible. The most significant errors occur if the untilted sample surface is misaligned from the horizontal about the tilt axis by an angle (α). On tilting for EBSD, the real specimen tilt is now $70° \pm \alpha$ and the raster scan in the y-direction which is inversely proportional to the tangent of this angle is substantially altered. For misalignments (α) of 1°, 2° and 5° the errors in the magnitude of the y-scan are 5%, 13% and 35% respectively, and thus it is concluded that accurate sample alignment is a critical factor if accurate grain or subgrain sizes are to be obtained.

3.2.4. Measuring subgrains—the limitations of angular precision

The improvement in EBSD spatial resolution obtainable from a FEGSEM mean that the sizes and size distribution of grains or subgrains as small as ~0.1–0.2 μm can be determined and this make the technique viable for most deformed metals. However, if such substructures consist primarily of subgrains of small misorientation, limitations may be placed upon EBSD analysis by the inaccuracies in the acquisition and analysis of electron backscatter patterns which were discussed in Section 2.2.4. This is well illustrated by a recent comparison of TEM and EBSD investigations of aluminium deformed to moderate strains, in which it was shown that the lower angle boundaries were not detected by EBSD [39]. In summary, the smallest misorientations

between grains or subgrains which can be determined by automated EBSD are typically between 0.5° and 1.5°. However, the lower limit is achievable only from very high quality patterns using a well calibrated system. This limit will be lowered when higher resolution cameras are employed and when more accurate algorithms for pattern measurement are developed. Individual diffraction patterns and hence misorientations may be measured with substantially better accuracy than this by measuring the relative positions of points from two overlapping patterns [26] which are recorded on a single image. However, this procedure has not yet been incorporated into automated commercial data acquisition systems, and for the metallographic applications discussed in this paper, only rapid and fully automated pattern acquisition and analysis method are relevant.

Because the orientation of each grain or subgrain is measured several times in an orientation map, some improvement in angular resolution may be achieved at the expense of spatial resolution by data processing. In a typical orientation map such as shown in Fig. 6a, there are a considerable number of data points in each grain, and the orientation of a grain could be more precisely defined if averaging of the data within a grain were to be carried out. The potential benefits of such a process can be determined from a simple statistical analysis. If the accuracy of a single orientation measurement is 1°, then the 95% confidence limit in the orientation of a grain will fall with the number (n) of pixels averaged, as $n^{-1/2}$. Orientation averaging is only valid if the true orientation is constant within each grain or subgrain, and this should be considered before such procedures are used. In annealed samples, this is generally a good assumption, but in materials containing many free dislocations and only poorly developed boundaries, orientation averaging would not be appropriate.

It is not a trivial matter to average orientations because although only three independent angular parameters are required to define a rotation, and so an orientation, in three spatial dimensions, there is no set of such parameters which facilitate operations such as orientation averaging in a satisfactory way. The problems associated with the statistical analysis of orientation data and various possible methods of orientation averaging are reviewed and discussed by Krieger Lassen *et al*. [40], Humbert *et al*. [41] and Humphreys *et al*. [42]. The use of the four Euler-symmetric parameters (often referred to as the quaternion description, though they are only coefficients of a quaternion) appears to be the best solution, particularly if only orientations spread over a range of a few degrees are to be averaged [41, 42], and this has recently been applied to EBSD maps [42]. Simple orientation averaging is not adequate as this would remove the boundaries, and it is necessary to incorporate an edge preserving routine such as the Kuwahara filter [43].

Fig. 11 shows an example of orientation averaging applied to part of an EBSD map from an Al-0.1wt% Mg alloy deformed 20% by cold rolling and annealed at 200°C. Fig. 11a shows the raw EBSD data. The subgrains are coloured according to their orientation relative to a reference pixel in the map. The subgrains are visible, but the data are noisy. If low angle grain boundaries of misorientations larger than 0.5° are superimposed on the map as in Fig. 11b, then it is seen that many of the "boundaries" lie inside the subgrains. Fig. 11c shows the effect of two passes of a modified Kuwahara filter on the raw data. The orientation noise is significantly reduced and the subgrains are more clearly visible. In Fig. 11d, the low angle grain boundaries $>0.5°$ are superimposed on the map and in contrast to Fig. 11b, the detected boundaries clearly match the microstructure. The subgrain sizes, shapes and misorientations and their distributions may be retrieved rapidly and automatically from the processed data of maps such as Fig. 11, and Fig. 12 is an example of the extensive information about subgrain size and misorientation distributions which can be obtained.

In analysing subgrain structures, the choice of technique is between EBSD or TEM. EBSD can analyse subgrains of a fraction of a micron in diameter, and, with orientation averaging, it can resolve low angle grain boundary misorientations of $\sim$0.5°, and several thousand subgrains may be analysed from a single map. The TEM can be used to image even the smallest subgrains, and subgrain misorientations of 0.1° can be determined. However, the numbers of subgrains which can be seen in a TEM thin foil is much less than can be determined in a solid SEM. Semi-automated methods for pattern analysis are available [7, 45] but these may take up to $\sim$60 seconds per pattern and a data set of more than 100 patterns from a sample is unusual [e.g. 46]. The techniques used for automated EBSD pattern analysis have been applied to the analysis of TEM diffraction patterns [7, 47, 48, 49], but it has proved more difficult to implement them for routine use [7, 48]. In selecting the most appropriate technique, the microscopist must therefore give serious consideration to the nature of the sample, the importance of including low angle grain boundaries of less than $\sim$0.50°, and the scale of the grain or subgrain structure.

4. The additional information available from EBSD

In Section 3, the use of EBSD for basic characterisation of grain and subgrain structures was discussed and it was concluded that in many cases there were significant advantages in using EBSD rather than standard metallographic methods for such analyses. However, there is a substantial amount of additional data available from EBSD maps, which is not available by other methods, and this will be highlighted in this section. This additional information is mainly related to the orientations of the grains and subgrains and to the character of the boundaries.

4.1. Microstructure and texture

The use of EBSD allows much more detailed grain characterisation than that discussed in Section 3 and in particular the relationships between the sizes and shapes of the grains and subgrains and their crystallographic orientation or **texture** can be determined. The orientations within a polycrystalline material which has undergone thermomechanical processing are usually far

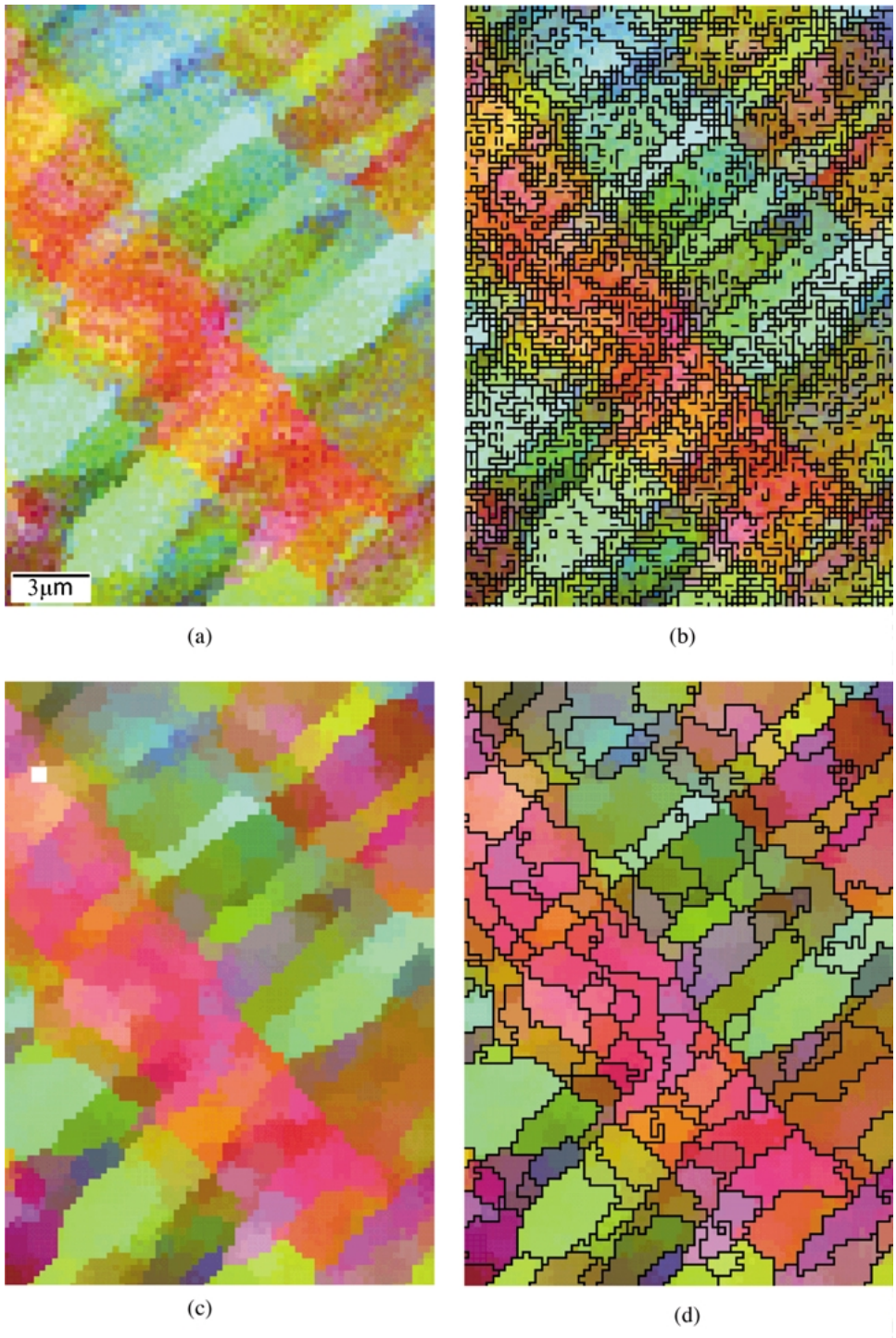

Figure 11 The effect of orientation averaging on the reduction of orientation noise in an EBSD map of a deformed and recovered aluminium alloy. (a) Raw data, (b) Raw data with boundaries $>0.5^\circ$ superimposed. (c) Data after two passes of modified Kuwahara filter. (d) Processed data with boundaries $>0.5^\circ$ superimposed [42].

from random, and the texture of such a material may often be considered to comprise several **ideal texture components** [e.g. 7, 50–52]. Because the mechanical and physical properties of a material are related to the texture, there is great interest in the control of texture during processing. As the orientation on each pixel in an orientation map is known, it can be checked against the various ideal texture components and if sufficiently close (typically within 15°), designated as belonging to that texture component. Analysis of the data of figure 4 shows that the only significant texture components are *Cube* {100}⟨001⟩ 9%, *Goss* {011}⟨100⟩ 3%, and *Brass* {110}⟨211⟩ and in Fig. 6b, the grains of these orientations are highlighted. In addition to the amounts of the texture components we can determine the grain sizes, shapes and subgrain misorientations for each texture component.

4.1.1. Bulk texture determination by EBSD

Textures are conventionally determined by the analysis of pole figures which are obtained from a sample by x-ray diffraction, and quantitative orientation distributions (ODFs) are obtained from analysis of 3–4 pole

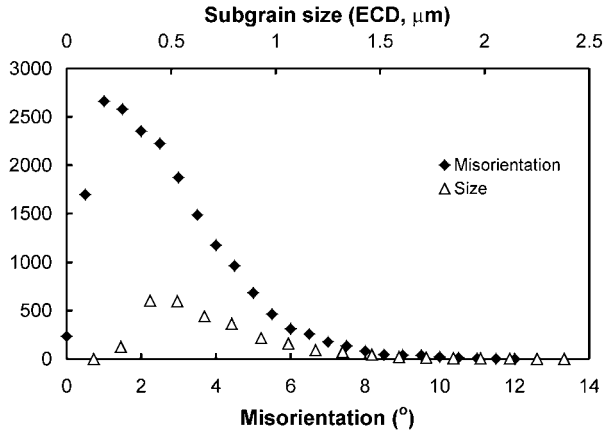

Figure 12 Distribution of subgrain sizes and misorientations in an Al-0.1%Mg alloy cold rolled 75%. showing the large amount of data available from an EBSD map [44], (Courtesy of P. J. Hurley).

figures. Such procedures are fully automated and as the time to obtain a single pole figure is typically ∼1.5 hrs the data acquisition time for a specimen is ∼4–6 hrs. There are certain errors in the experimental x-ray procedures such as line broadening [7, 51] and in the data analysis (e.g. ghost peaks), which lead to inaccuracies in calculating orientation distribution functions by the deconvolution of pole figures, and one of the original reasons for the development of fully automated EBSD analysis was to eliminate such errors by obtaining the crystallographic texture of a specimen directly from individual diffraction patterns [15, 32].

The experimental method of obtaining a "bulk" texture from a sample by EBSD is relatively straightforward. The sample, which should be representative of the bulk material, is often polished on the RD-ND plane because in rolled material this section samples the microstructure better than the rolling plane. A specimen which is 15 mm in the rolling direction, cut from 3 mm sheet in a material of grain size 100 μm would reveal ∼5000 grains on its surface. Diffraction patterns are obtained from a grid of points covering the entire specimen or a selected region. From these data the orientation distributions are obtained and these can be displayed as pole figures or ODFs in Euler space, or alternatively the fraction of material approximating to selected ideal texture components may be calculated. If a texture representative of the bulk material is to be obtained then it is important that data is obtainable from all parts of the microstructure. A heavily deformed material may contain cells or subgrains which are below the resolution of a W-filament SEM, and this may result in an unacceptably low fraction of indexed diffraction patterns. In addition, if the cell size depends on grain orientation (e.g. Table IV), certain orientations will be sampled more efficiently than others and measured texture will be incorrect. For such materials, it may be necessary to used a FEGSEM to achieve an acceptable level of pattern solution.

If the technique described above is used to determine the texture of a suitably representative specimen then the number of data points required to produce a statistically significant orientation distribution function needs consideration. Experiments have shown that the number of orientation determinations required is in the range 500–1500 [32, 53]. If these individual orientations are used directly, then the pole figures or orientation distribution functions are noisy. The data is therefore usually smoothed by convolution with a Gaussian of half width 1–5°. The amount of smoothing for optimum fit with conventional x-ray data remains a matter of debate, but for a given material is usually determined by experiment [32, 53]. Such a texture determination using 1000 points and carried out by stage scanning will take only ∼20 minutes, which should be compared with the 4–5 hrs required for x-ray analysis. We therefore conclude that for suitable materials, bulk texture determination by EBSD may offer a significant time saving over conventional x-ray analysis.

In many rolled materials the deformation or recrystallization textures vary through the sheet thickness [e.g. 54]. In such circumstances, suitable data grids on a single ND-RD section specimen may be analysed by EBSD to provide through-thickness texture data in a fraction of the time which would be required for conventional x-ray analysis of several specimens sectioned parallel to the rolling plane and ground to the required depths.

The spatial distribution of texture components within a sample may also be important. For example undesirable ridges may occur on the surface of drawn metal sheet and these are known as "roping" in aluminium alloys and "ridging" in steels. EBSD has been used to investigate these effects and it is now believed that they are associated with the spatial distribution of certain texture components [55]. An EBSD map may be analysed to determine the size and spacing of concentrations of particular texture components, using fourier transform methods, and Lee *et al*. [56] have defined a "disorientation correlation function" which quantifies the spatial distribution of texture.

4.1.2. Texture and substructure

In addition to determining the subgrain size, shape and misorientation, EBSD allows correlation of these parameters with the orientation. The analysis of a hot-deformed aluminium alloy provides a good illustration of the power of the technique. Fig. 13 is an orientation map from a specimen of a typical hot-worked commercial aluminium alloy in which both the elongated original grains and the subgrains are seen. The high and low angle boundaries are easily differentiated during analysis of the data as is shown in Fig. 13a. The EBSD data may be analysed to obtain the mean size and shapes of the grains and subgrains as shown in Table III (the data for which were obtained from a larger area of the same sample). However, in addition, EBSD reveals correlations between size and orientation, orientation and misorientation or size and misorientation as shown in Table IV. From this table we can see that the "cube" oriented subgrains are not only larger than those of other orientations but they also have a larger mean misorientation to their neighbours. Such detailed information is invaluable in interpreting the behaviour of deformed alloys during subsequent annealing [e.g. 46]. There is

TABLE III Grain and subgrain sizes from EBSD data from the specimen of Fig. 13

	Grains		Subgrains	
	Mean	Std err	Mean	Std err
Number	379		1356	
Diameter (μm)	4.23	0.23	2.47	0.05
X-length (μm)	6.68	0.59	2.95	0.09
Y-length (μm)	3.33	0.15	2.18	0.04

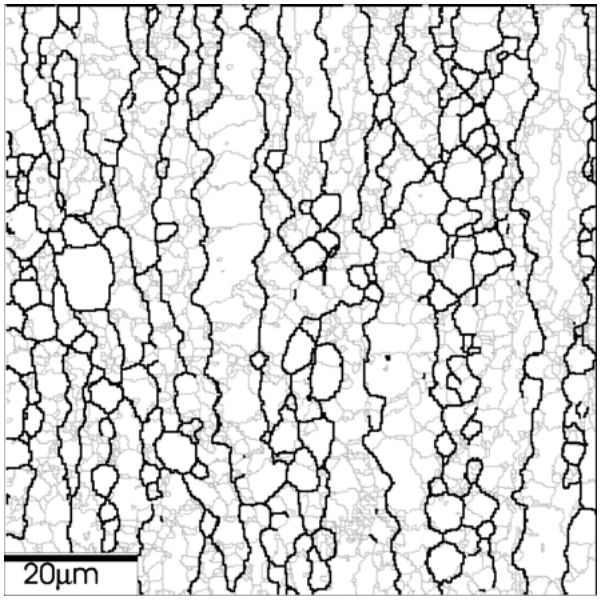

(a)

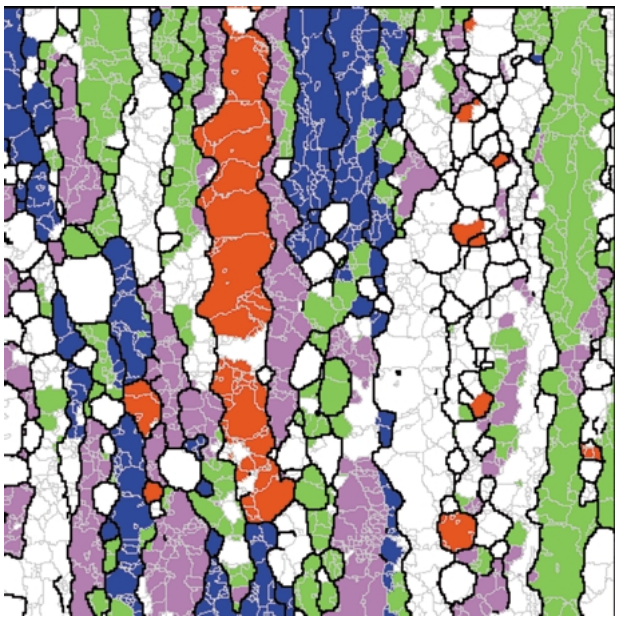

(b)

Figure 13 Orientation map from a commercial Al-Mg alloy (AA5182), deformed by plane strain compression at 350°C and sectioned in the RD-ND plane. (a) High angle boundaries shown as black and low angle boundaries as grey. (b) Regions within 15° of the main texture components are shaded – Cube {001}⟨100⟩ red, Brass {011}⟨112⟩ blue, S {123}⟨634⟩, green, Copper {112}⟨111⟩ purple), with other areas in white.

a great deal more information about grains and subgrains which may easily be obtained from an orientation map. For example, correlations between subgrain size and misorientation during recovery have been used to determine the mobility of low angle boundary mobilities [57].

TABLE IV Subgrain sizes, orientations and misorientations from EBSD data from the specimen of Fig. 13

Texture component	Number	Diameter μm	Mean misorientation (o)	Texture fraction
Brass {011}⟨211⟩	112	2.48	5.67	0.13
Copper {112}⟨111⟩	138	2.43	5.04	0.16
Cube {001}⟨100⟩	81	3.01	6.69	0.08
Goss {011}⟨100⟩	80	2.22	6.11	0.01
P {011}⟨122⟩	1	1.79	—	0
S {123}⟨634⟩	344	2.58	5.16	0.35

4.1.3. Stored energy

Although the spatial and angular resolutions of EBSD are currently insufficient to resolve information about individual dislocations, lattice misorientations and orientation gradients may be measured and hence information can be obtained about the geometrically necessary dislocation content of the material [11]. If the dislocation substructure is in the form of subgrains of diameter D and boundary energy γ then the stored energy of the material (E) can be taken as [50].

$$E = \frac{K_1 \gamma}{D} \tag{7}$$

where K_1 is a geometric constant ~3.

If the subgrain structure is reconstructed from EBSD data, the subgrain sizes and misorientations may be determined and thus the local stored energy calculated. A measure of the spatial distribution of stored energy in the sample can then be represented as a "stored energy map" as shown in Fig. 14b. An alternative method of determining the spatial distribution of stored energy is to determine the misorientation of a pixel from its neighbours and for each pixel calculate a mean boundary energy. The sum of the boundary energy over the map then enables the stored energy of the map area to be determined, and again, the spatial distribution of the energy can be represented as a map.

The deformed sample of Fig. 14 has an inhomogeneous microstructure, and in particular shows "deformation bands" (**B**) within grains such as **A**. The stored energy map of Fig. 14b shows that the stored energy varies through the microstructure and in particular, that the deformation bands have larger stored energies than the remainder of the grain. Analysis of the stored energy map shows that the mean stored energy in the sample is 0.38 MJ m^{-3}, the stored energy in region A is ~0.27 MJ m^{-3} and in region B is ~0.45 MJ m^{-3}.

4.2. Boundary character

Some of the most important parameters which can be determined from EBSD are related to the nature of the grain boundaries. A boundary is characterised by five degrees of freedom, three of which relate the orientation of the material either side of the boundary and

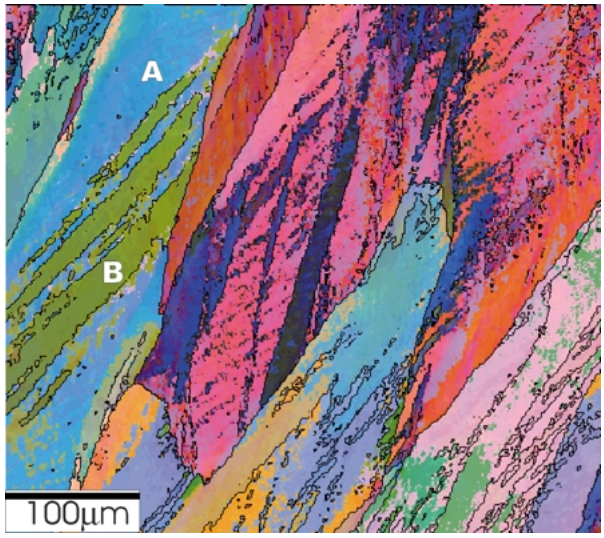

(a)

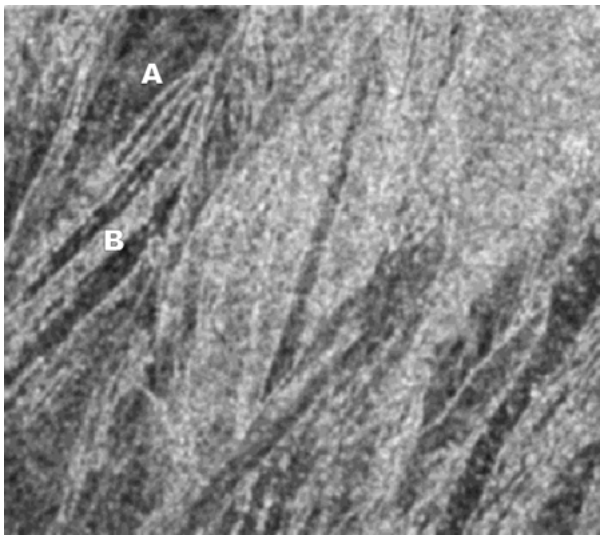

(b)

Figure 14 EBSD map of Al-0.13%Mg deformed to a strain of 1.3 by Equal Channel Angular Extrusion, showing inhomogeneous deformation. (a) Euler colour map with high angle boundaries marked in black. (b) Stored energy map in which the grey level is proportional to the local stored energy. (Map data courtesy of J. Bowen).

two degrees of freedom which define the inclination of the plane of the boundary.

4.2.1. Misorientation and disorientation

Once a boundary is detected in an EBSD map, the angular relationship between the crystals associated with the boundary is readily calculated because the orientations of the crystals are known (within the experimental errors discussed in Section 3.2). This relationship may be expressed in terms of the **rotation matrix** [e.g. 7, 51, 58], the **Rodrigues vector** [59], or more commonly as an **angle-axis pair**. The last method, which is used in this paper, defines the angle by which one of the crystals must be rotated about a particular axis so as to bring it into register with the other crystal. In a cubic crystal there are 24 possible solutions, and in the absence of any special sample symmetry, it is conventional to describe the relationship between the grains as the angle/axis pair associated with the **smallest** rotation [31] and this is often termed the **disorientation**. It should be noted that misorientations other than the disorientation may sometimes be appropriate [60].

4.2.2. The boundary plane

The other two degrees of freedom describing the boundary plane are less readily determined. One of these parameters is obtainable from the direction of the boundary in the map, but the other parameter, which is the inclination of the boundary to the surface of the sample, is not directly obtainable. For large grains, the boundary plane may be determined by sectioning and examining the sample in two orthogonal planes [7, 61], or in the more general case, by serial sectioning in which the sample is measured after controlled etching [62–64]. The crystallography of free boundary planes such as fracture surfaces may also be determined by EBSD [e.g. 12, 65]

4.2.3. The distribution of boundary angles

EBSD data may be processed so as to display the character of the boundaries, and a simple case is shown in Fig. 6c where boundaries designated high angle ($>15^\circ$) are shown in black, and low angle ($<15^\circ$) are grey. The distribution of boundary angles is also obtainable, and Fig. 6e shows a histogram of the distribution of grain boundary misorientation, sometimes called a McKenzie plot [31] for the specimen of Fig. 6. The shape of this distribution and the mean boundary misorientation of 40.3° is close to the value of 40° which would be found for a randomly oriented assembly of grains [31]. Parameters such as the mean boundary misorientation and fraction of high angle boundaries (0.97) which are obtainable from EBSD data may be as relevant to the properties of the material as is the grain size, and EBSD allows such parameters to be readily measured.

Recent research on the production of sub-micron-grained alloys by thermomechanical processing provides a good illustration of the application of EBSD boundary characterisation. It has been shown that after plastic deformation to very large strains, followed by low temperature annealing, many alloys develop a relatively stable micron-scale grain structure [e.g. 66–70]. In order to distinguish between a true micron-grained microstructure and a microstructure comprising mainly micron-sized subgrains, it is necessary to determine the nature of the grain boundaries.

Selected area diffraction patterns in the TEM from such materials generally exhibit arcing, which indicates that the material contains large orientation gradients within the selected area. Such observations give no indication as to boundary character, and do not prove, as has been claimed [e.g. 67] that the majority of the grain boundaries are high angle. However, detailed boundary characterisation can be readily obtained from EBSD maps [68–70], and Fig. 15, shows how EBSD may be used to determine the relative amounts of high angle and low angle boundary as a function of the deformation strain, thus enabling the processes involved in the microstructural evolution to be clarified.

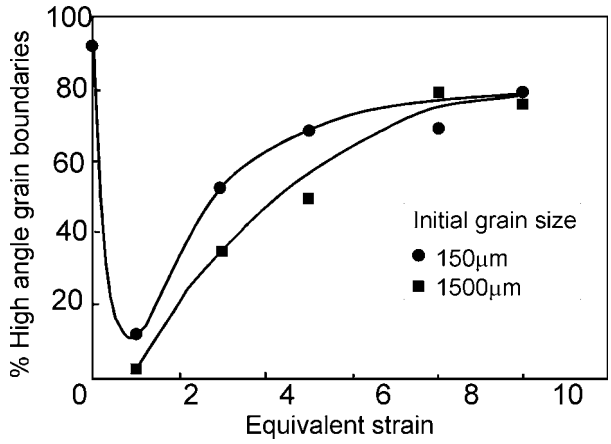

Figure 15 The percentage of high angle boundaries as a function of strain in AA1050 deformed by Equal Channel Angular Extrusion [68].

4.2.4. Special boundaries

EBSD analysis can determine the complete orientation relationship at a grain boundary and therefore more information than the misorientation angle, which was discussed in the preceding section, is available. For example it is possible to detect and measure boundaries which have special orientation relationships, such as coincidence site lattice (CSL) boundaries [71] in which there is good atomic matching across the boundary and a significant fraction of the atom sites are common to both crystals. The reciprocal of the ratio of atom sites which are common to both crystals (coincidence sites) to lattice sites is denoted by Σ. For example, in a twin boundary in fcc material, one third of the lattice sites are common to both crystals and this is therefore a $\Sigma 3$ boundary. Detailed tables of the orientation relationships for CSL boundaries are given by Mykura [72] and shorter tables are found in several books [e.g. 7, 50].

In order to determine whether a measured boundary can be classified as a CSL boundary, some criterion as to the allowable deviation from the exact orientation relationship must be used, and the **Brandon criterion** [73] is most commonly used. This states that the maximum allowable misorientation ($\Delta\theta$) from the exact CSL relationship is

$$\Delta\theta = \theta_m \Sigma^{-1/2} \tag{8}$$

where θ_m is the maximum misorientation angle for a low angle boundary (typically 15°). Thus for a low angle boundary ($\Sigma 1$), $\Delta\theta = 15°$ and for a $\Sigma 3$ boundary, $\Delta\theta = 8.7°$. It has been suggested that this criterion is too broad and that a $\Sigma^{-5/6}$ dependency is more appropriate [74]. More detailed discussion of CSL boundaries may be found in the references cited in this section.

Fig. 16 is an orientation map of a recrystallized α-brass sample. In figure 16b the $\Sigma 3$ boundaries are shown in red, $\Sigma 9$ boundaries in green and other boundaries in black. Analysis of the data shows that the microstructure contains 2% of low angle ($\Sigma 1$) boundaries, 67% of $\Sigma 3$ twin boundaries and 5% of the higher order $\Sigma 9$ twin boundaries. These figures are length-related boundary frequencies, but number-related frequencies are also obtainable if grain reconstruction is used.

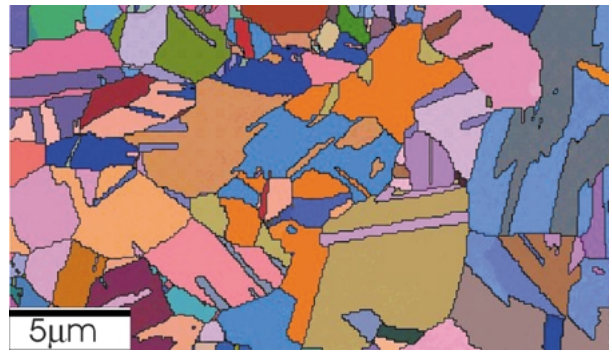

(a)

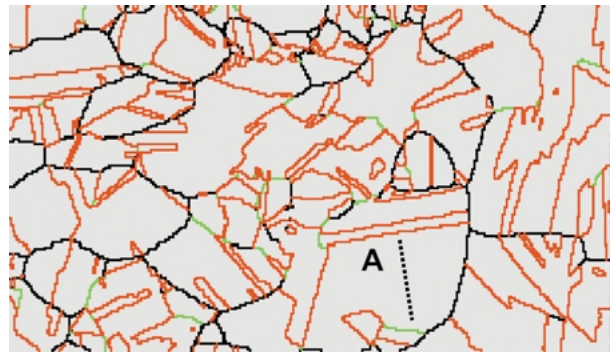

(b)

Figure 16 EBSD map of a fine-grained recrystallized α-brass specimen. (a) Orientation map (Euler contrast), with high angle grain boundaries are shown as black lines. (b) Twin ($\Sigma 3$) boundaries shown as red, $\Sigma 9$ boundaries as green and other boundaries as black.

Certain low Σ boundaries may have special properties (see below), if they also lie on specific planes. A well known example of this is found for $\Sigma 3$ boundaries, where the coherent boundaries which lie on the {111} twinning plane have much lower energies and mobilities than the incoherent twin boundaries on other planes, leading to their characteristic planar habit seen in Fig. 16. This is an example of a case where knowledge of the boundary plane is required in addition to the misorientation. Although, as discussed above, the boundary plane cannot be fully determined from a single EBSD map, some information may be obtained from the trace of the boundary. For example, in Fig. 16b, measurement of the boundary at **A** shows it to have a 60° misorientation about a ⟨111⟩ axis, which is a $\Sigma 3$ relationship. The trace of this rotation axis, (dotted line in Fig. 16b), is perpendicular to the trace of the boundary, and this is consistent with the boundary being parallel to the twinning plane, i.e. a coherent twin boundary, although of course it is not conclusive proof.

4.2.5. Grain boundary engineering

There is evidence that particular types of boundaries such as coincidence site lattice (CSL) boundaries are less susceptible to damage such as creep cavitation or corrosion than normal boundaries, and the concept of **Grain Boundary Engineering** in which the material is processed to maximise the number of CSL boundaries in order to optimise properties has gained prominence in recent years [74–77]. EBSD is an essential tool in measuring the amount of CSL boundary and Fig. 17, from the work of Ardakani and colleagues [78]

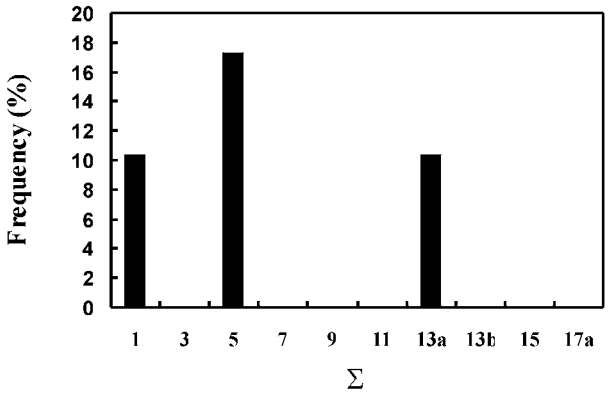

Figure 17 Distribution of coincident site lattice (CSL) boundaries in a directionally solidified nickel superalloy [78]. (Courtesy M.G. Ardakani).

shows the fraction of CSL boundaries formed during controlled solidification of a nickel superalloy which is being developed for creep resistance. The numbers of CSL boundaries in this sample are much larger than in a random grain assembly where the numbers of $\Sigma 1$, $\Sigma 5$ and $\Sigma 13a$ boundaries would be 2.2%, 1.2% and 0.3% respectively [79].

5. Estimating recrystallization from EBSD data

The characterisation of fully recrystallized materials and deformed materials has been discussed in previous sections. There is also interest in following the progress of recrystallization, and in particular in determining the fraction of the microstructure which has recrystallized. When examining deformed and annealed samples, the fraction recrystallized is normally determined by optical metallography [e.g. 80]. However, there are several methods by which this information may be obtained from EBSD.

5.1. The fraction of indexed patterns

The unrecrystallized regions of a sample contain dislocations, cells or subgrains [50]. If the deformed regions are such that an analysable pattern cannot be obtained from them, this could be used as a criterion to distinguish the recrystallized regions and thus obtain a measure of the fraction recrystallized. Such a method relies on the region sampled by the beam being sufficiently defective so as not to produce an analysable pattern. This method will not work if the material contains subgrains larger than the area sampled by the beam ($\Lambda_A \times \Lambda_P$) and is therefore rarely suitable for most aluminium alloys or hot deformed materials. Even in non-cell forming metals such as stainless steel and brass which have been cold deformed to large strains, analysable patterns will be produced in some deformed regions, depending on the crystallography of the local deformation and our attempts to use this method have not produced reliable results.

5.2. The pattern quality

An alternative approach is based on the assumption that the quality (sharpness or contrast) of the diffraction patterns will be different for recrystallized and non-recrystallized regions. A semi-automated version of this method has been successfully used to differentiate between deformed and recrystallized area in steels [81], and the use of automated methods has been proposed [82–84]. However, there are several problems automating such a method:

- The pattern quality is not necessarily a good measure of the defect density and even in recrystallized grains, pattern quality depends on crystallographic orientation (see Fig. 18a)
- The method requires calibration for each type of sample
- Pattern quality is lower in boundary regions (Fig. 2b) because of overlapping patterns, and grain boundaries cannot readily be distinguished from defective grain interiors.
- A diffraction pattern comes from the region of beam interaction (Fig. 3). If the cell or subgrain size is smaller than this, a poor quality pattern results and vice versa. Therefore the pattern quality depends not only on the sample, but also on the EBSD spatial resolution (Section 2.2.3). Thus the pattern quality for a given sample will be better in a FEGSEM than a W-filament SEM and will be sensitive to beam defocus etc.

The two methods described above both have the advantage that comparatively little data are required in order to analyse the microstructure. They may be used as point counting methods, similar to that used for optical microscopy [80], where a coarse grid of points is obtained and each point is analysed to determine whether it corresponds to a recrystallized or unrecrystallized region. The number of data points required for an accurate analysis depends on the number and size of the recrystallized grains, and is typically 500–600 [80]. Such an analysis would take only 2–3 minutes with beam scanning and ~10 minutes with stage scanning.

5.3. From high resolution EBSD linescans

An alternative approach is to achieve a high success rate of pattern solving, obtain data at a spatial resolution which is less than the subgrain size and subsequently analyse the data to determine the grain boundary characteristics [21]. This method is applicable to materials which have well-defined subgrain structures which are larger than the effective spatial resolution of EBSD, and good results have been obtained from a number of aluminium samples including hot deformed AA5xxx and AA6xxx alloys. An EBSD linescan is obtained and the data are subsequently analysed to identify high angle and low angle boundaries. The method is somewhat similar to that discussed in Section 3.1.1 for grain size analysis, but differs because the character of adjacent boundaries is examined. If during this one-dimensional analysis, two adjacent low angle boundaries are detected then the material between them is considered to be a subgrain. A region bounded by a high and a low angle boundary is also considered to be a subgrain. However a region bounded by two high angle boundaries is considered to be a grain. In this way, the microstructure

is divided into grains and subgrains and the proportion of grains in the material can be taken to be the fraction recrystallized. This method of analysis has the advantage over conventional optical metallography in that it can measure the early stages of recrystallization, and that it is fully automatic, requiring no interpretation by the operator. The time to acquire data depends on the heterogeneity of the microstructure, the amount of recrystallization, the size of the subgrain structure and the accuracy required. For example, for 5 μm subgrains, a scan step of $\sim$1 μm is appropriate and for a data linescan of total length 10 mm, some 10,000 data points are required, This would take $\sim$2–3 hrs by stage scanning or $\sim$30 minutes by beam scanning.

5.4. From high resolution EBSD maps

A more accurate but considerably slower method of analysing the microstructure is to acquire an EBSD map with a step size smaller than the subgrain size (Fig. 18). After grain and subgrain reconstruction the boundaries surrounding all the grains and subgrains can be examined. A quantitative definition of a recrystallized grain is then required, and on this basis all regions can be classified as either recrystallized or non-recrystallized [21].

Examining the microstructure in such detail gives rise to the interesting decision as to how a recrystallized region should be formally differentiated from an unrecrystallized region, and no clear answer can be given. We can define a region as being recrystallized according to one or more of the following criteria:

- A region bounded by a certain fraction (0–1) of high angle boundaries
- A region which is larger by a given factor (e.g. 4) than the cells or subgrains
- A region where the pattern quality is greater than a certain fraction (e.g. 0.5) of the mean.

In Fig. 18b, a recrystallized grain has been defined as being a region which has at least one high angle boundary and is at least 4x larger than the subgrain size, and analysis gives the result that the sample is 42% recrystallized with a mean recrystallized grain size of 7.7 μm and that 11% of the recrystallized grains are of the cube orientation. It should be emphasised that such high resolution EBSD maps are unlikely to become an economical method of estimating the recrystallized fraction. However, they are invaluable aids to analysing the evolution of microstructures and textures during annealing.

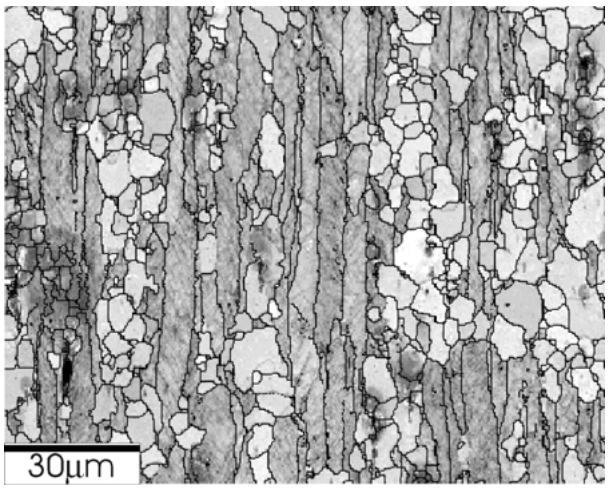

(a)

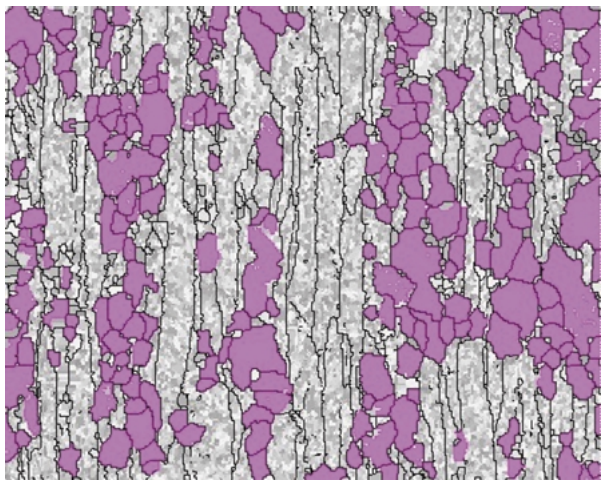

(b)

Figure 18 EBSD map of hot-deformed and partly recrystallized Al–Mg alloy (AA5182). (a) Pattern quality map in which the high quality patterns appear brighter, with high angle boundaries superimposed. (b) As (a), but the regions define as being recrystallized are coloured.

6. Conclusions

1. The technique of EBSD has reached a state of maturity such that EBSD linescans and maps can be routinely obtained and analysed using commercially available equipment. EBSD in a FEGSEM allows quantitative analysis of grain/subgrains as small as $\sim$0.2 μm.

2. Automated EBSD can result in more accurate measurements of grain and subgrain size than conventional imaging methods, often in comparable times.

3. Subgrain/cell measurements may be made more easily than in the TEM. The limited angular resolution of EBSD may be problematic for subgrains of low misorientation, although this can be reduced by data processing.

4. Additional information available from an EBSD map includes texture and its correlation with grain or subgrain size, shape and position.

5. EBSD may rival X-ray methods for determining bulk texture.

6. Boundary misorientations, which are readily obtainable from EBSD, enable the distribution of boundary character to be determined. CSL boundaries can be identified and measured.

7. Recrystallization and stored energy may be measured by EBSD methods.

Acknowledgments

The author wishes to acknowledge the financial support of EPSRC and Alcan International for the development of the EBSD facilities in the Manchester Materials Science Centre. The technical support provided by Ian Brough has been invaluable, as has been the enthusiasm of members of the Light Alloy Processing Group in the Centre.

References

1. British Standard BS4490:1989, British Standards Institute, London (1989).
2. E. E. UNDERWOOD, "Quantitative Stereology" (Addison-Wesley, Reading, MA, 1970).
3. B. HUTCHINSON, L. RYDE and E. LINDH, *Math. Sci. Eng.* **A257** (1998) 9.
4. H. S. UBHI, P. HOLDWAY, D. BAXTER and S. PITMAN, DERA, Farnborough (private communication).
5. F. J. HUMPHREYS, in "Quantitative Microscopy of High Temperature Materials," edited by A. Strang (Institute of Materials, in press).
6. A. J. WILKINSON and P. B. HIRSCH, *Micron* **28** (1997) 279.
7. V. RANDLE and O. ENGLER, "An Introduction to Texture Analysis" (Gordon and Breach, Amsterdam, 2000).
8. M. N. ALAM, M. BLACKMAN and D. W. PASHLEY, *Proc. Royal Soc. Lond.* **A221** (1954) 224.
9. D. J. DINGLEY and V. RANDLE, *J. Mater. Sci.* **27** (1992) 4545.
10. V. RANDLE, "Microtexture Determination" (Institute of Materials, London, 1992).
11. B. L. ADAMS, *Ultramicroscopy* **67** (1997) 11.
12. D. P. FIELD, *ibid.* **67** (1997) 1.
13. S. I. WRIGHT and B. L. ADAMS, *Metall. Trans* **23A** (1992) 759.
14. N. C. KRIEGER LASSEN, D. JUUL JENSEN and K. CONRADSEN, *Scanning Microsc.* **6** (1992) 115.
15. B. L. ADAMS, S.I. WRIGHT and K. KUNZE, *Met. Mat. Trans.* **24A** (1993) 819.
16. F. J. HUMPHREYS and I. BROUGH, *J. Microscopy* **195** (1999) 6.
17. D. J. PRIOR, P. W. TRIMBY, U. D. WEBER and D. J. DINGLEY, *Mineral. Mag.* **60** (1996) 859.
18. A. P. DAY and T. E. QUESTED, *J. Microscopy* **195** (1999) 186.
19. J. R. MICHAEL, *Microsc. Microanal.* **5** (1999) 218.
20. F. J. HUMPHREYS (2000). **VMAP** is a suite of programmes developed for quantitative analysis of the EBSD data generated by the **HKL Channel** acquisition system. It can be made available on request.
21. *Idem., J. Microscopy* **195** (1999) 170.
22. T. PETTERSEN, G. HEIBERG and J. HJELEN, in Proc. ICEM 14, Cancun, Mexico, **3** (1998) 775.
23. F. J. HUMPHREYS, Y. HUANG, I. BROUGH and C. HARRIS, *J. Microscopy* **195** (1999) 212.
24. J. L. GOLDSTEIN, D. C. JOY, A. D. ROMIG, C. E. LYMAN, C. FIORI and E. LIFSHIN, "Scanning Electron Microscopy and X-ray Microanalysis" (Plenum, New York, 1992).
25. N. C. KRIEGER LASSEN, *J. Microscopy* **181** (1996) 72.
26. A. J. WILKINSON, in Proc. EMAG99. *Inst. Phys. Conf. Ser.* **161** (1999) 115.
27. D. J. PRIOR, *J. Microscopy* **195** (1999) 217.
28. K. KUNZE, B. L. ADAMS, F. HEIDELBACH and H. R. WENK, in 10th Int Conf. on Textures (ICOTOM10), edited by H. Bunge (Clausthal, Germany, 1993), 1243.
29. D. J. PRIOR, A. P. BOYLE, F. BRENKER, M. CHEADLE, A. DAY, G. LOPEZ, G. J. POTTS, S. REDDY, R. SPIESS, N. E. TIMMS, P. TRIMBY, J. WHEELER and L. ZETTERSTRÖM, *American Mineralogist* **84** (1999) 1741.
30. R. T. DE HOFF and F. N. RHINES, "Quantitative Microscopy" (McGraw Hill, New York, 1968).
31. J. K. MACKENZIE, *Biometrika* **45** (1958) 229.
32. S. I. WRIGHT and U. F. KOCKS, in Proc. 11th Int. Conf. on Texture, Xian, edited by Z. Liang (Int Academic Publishers, Beijing), **1** (1996) 53.
33. D. J. DINGLEY and D. P. FIELD, *Mater. Sci. Technol.* **13** (1997) 69.
34. R. L. FULLMAN, *Trans. AIME* **197** (1953) 447.
35. Y. HUANG and F. J. HUMPHREYS, *Acta Mater.* **48** (2000) 2017.
36. W. YANG, B. L. ADAMS and M. DE GRAEF, in Proc. 11th Int Conf. on Textures (ICOTOM11), edited by J. Szpunar, Montreal, (1999) 192.
37. B. L. ADAMS, in Proc. 11th Int Conf. on Textures (ICOTOM11), Montreal, edited by J. Szpunar, (1999) p. 9.
38. D. DYSON, *Proc. Royal Mic. Soc.* **35**(2) (2000) 147.
39. X. HUANG and D. J. JENSEN, in Proc. EBSD Seminar, TMS Fall meeting (2000), in press.
40. N. C. KRIEGER LASSEN, D. JUUL JENSEN and K. CONRADSEN, *Acta Crystall.* **A50** (1994) 741.
41. M. HUMBERT, N. GEY, J. MULLER and C. ESLING, *J. App. Cryst.* **29** (1996) 662.
42. F. J. HUMPHREYS, P. S. BATE and P. J. HURLEY, *J. Microsc.* (2000), in press.
43. M. KUWAHARA and S. EIHO, in "Digital Processing of Biomedical Images" edited by K. Preston and M. Onoe (Plenum Press, New York, 1976) p. 187.
44. P. J. HURLEY and F. J. HUMPHREYS, in Proc. 5th Int Conf. on Recrystallization, Aachen, edited by G. Gottstein and D. Molodov (2001), in press.
45. R. A. SCHWARZER and H. WEILAND, in Proc. 7th Int Conf. on Textures (ICOTOM7), Zwidjendrecht, edited by C. M. Brackman (Netherlands Soc. for Mats. Sci. 1984), p. 839.
46. A. BARDAL, I. LINDSETH, H. E. VATNE and E. NES, in Proc. 16th Riso Int. Symp, Denmark, edited by N. Hansen *et al.* (Riso National Laboratory, 1995), p. 261.
47. N. C. KRIEGER LASSEN, in Proc. 16th Riso Int. Symp, Denmark, edited by Hansen *et al.* (Riso National Laboratory, 1995), p. 405.
48. R. A. SCHWARZER, *Ultramicroscopy* **67** (1997) 19.
49. Q. LIU, *ibid.* **60** (1995) 81.
50. F. J. HUMPHREYS and M. HATHERLY, "Recrystallization and Related Annealing Phenomena" (Pergamon, Oxford, 1995).
51. H. J. BUNGE, "Texture Analysis in Materials Science" (Butterworth, London, 1992).
52. R. W. CAHN, in "Processing of Metals and Alloys," edited by Cahn (VCH, Heinheim, 1991), p. 429.
53. W. B. HUTCHINSON, E. LINDH and P. S. BATE, in Proc. 12th Int Conf. on Texture, edited by J. Szpunar (NRC Press, Ottawa, 1999), p. 34.
54. A. W. BOWEN, *Mater. Sci. Tech.* **6** (1990) 1058.
55. G. J. BACZYNSKI, R. GUZZO, M. D. BALL and D. J. LLOYD, *Acta Mater.* **48** (2000) 3361.
56. P. S. LEE, A. D. ROLLETT and B. L. ADAMS, in Proc. ICOTOM12, 1999, p. 21.
57. Y. HUANG, F. J. HUMPHREYS and M. FERRY, *Acta Mater.* **48** (2000) 2543.
58. J. HANSEN, J. POSPIECH and K. LUCKE, "Tables for Texture Analysis of Cubic Crystals" Springer-Verlag, Berlin (1978).
59. F. C. FRANK, *Metall. Trans.* **19A** (1988) 403.
60. W. B. HUTCHINSON, L. RYDE, P. S. BATE and B. BACROIX, *Scripta Mater* **35** (1996) 579.
61. V. RANDLE, "The Measurement of Grain Boundary Geometry" (Inst. Phys. Publishing, Bristol, 1993).
62. B. ADAMS, D. KINDERLEHRER, W. W. MULLINS, A. D. ROLLETT and S. TAASAN, *Scripta Mater.* **38** (1998) 531.
63. C.-C. YANG, A. D. ROLLETT and W. W. MULLINS, in Proc. 21st Riso Int. Symp., Denmark, edited by N. Hansen *et al.* (Riso National Laboratory, 2000), p. 659.
64. V. RANDLE, M. CAUL and J. FIEDLER, *Micros. Microanal.* **3** (1997) 224.
65. V. RANDLE and C. HOILE, in Proc. Int. conf. on Texture and Anisotropy of Polycrystals, edited by R. Schwarzer (Trans Tech Publishing, Switzerland, 1998), p. 183.
66. V. M. SEGAL, *Mater. Sci. Eng.* **A197** (1995) 157.
67. K. NAKASHIMA, Z. HORITA, M. NEMOTO and T. G. LANGDON, *Acta Mater.* **46** (1998) 1589.
68. C. HARRIS, P. B. PRANGNELL and X. DUAN, in Proc. 6th Int. Conf on aluminium alloys (ICAA6), edited by T. Sato *et al.* (Toyohashi, Japan) **1** (1998) 583.
69. F. J. HUMPHREYS, P. B. PRANGNELL, J. R. BOWEN, A. GHOLINIA and C. HARRIS, *Phil. Trans. Royal Society* **A357** (1999) 1663.
70. A. GHOLINIA, P. B. PRANGNELL and M. V. MARKUCHEV, *Acta Mater.* **48** (2000) 1115.
71. D. G. BRANDON, B. RALPH, S. RANGANATHAN and M. S. WALD, *Acta Metall.* **12** (1964) 813.
72. H. MYKURA, in "Grain Boundary Structure and Kinetics," edited by Balluffi (ASM, Ohio, 1980), 445.

73. D. G. BRANDON, *Acta Metall*. **14** (1966) 1479.
74. G. PALUMBO and K. T. AUST, in "Materials Interfaces," edited by Wolf and Yip (Chapman and Hall, London, 1992), p. 190.
75. T. WATANABE, in Proc. 4th Int Conference on Recrystallization, edited by T. Sakai and H. Suzuki, Japanese Institute of Metals, Tsukuba, Japan (1999), p. 99.
76. V. RANDLE, "The Role of the Coincidence Site Lattice in Grain Boundary Engineering" (Inst. of Materials, London, 1996).
77. E. M. LEHOCKEY and G. PALUMBO, *Mater. Sci. Eng*. **A237** 168.
78. M. G. ARDAKANI, N. D'SOUZA, B. SHOLLOCK and M.MCLEAN, *Met. Trans A* **31A** (2000) 2887.
79. Y. PAN and B. L. ADAMS, *Scripta Metall*. **30** (1994) 1055.
80. P. L.ORSETTI ROSSI and C. M. SELLARS, *Acta Mater*. **45** (1997) 137.
81. E. LINDH, B. HUTCHINSON and P. BATE, in Proc. 10th Int Conf of Textures, 1995. Clausthal-Zellerfeld, Germany, edited by H. J. Bunge (Trans Tech Publications, Switzerland, 1993) p. 1917.
82. O. ENGLER, in Proc. 19th Riso Int. Symp. Denmark, edited by J. Carstersen *et al*. (Riso National Laboratory, 1998), p. 253.
83. M. P. BLACK and R. L. HIGGINSON, *Scripta Mater*. **41** (1999) 125.
84. S. I. WRIGHT, in Proc. 12th Int. Conf. on Texture, edited by J. Szpunar (NRC Press, Ottawa, 1999), p. 104.

Received 4 December
and accepted 19 December 2000